ALLEVIATING MITOCHONDRIAL MYOPATHY IN MICE

By
Semin Erkul
B.S., Molecular Biology and Genetics, Boğaziçi University, 2020

Submitted to the Institute for Graduate Studies in
Science and Engineering in partial fulfillment of
the requirements for the degree of
Master of Science

Graduate Program in Molecular Biology and Genetics
Boğaziçi University
2023

ACKNOWLEDGMENTS

All the wonderful people I would like to mention in this section, I am indefinitely grateful and fortunate to have you in my life and through my M.Sc. studies.

First, I wish to thank my supervisor, Assist. Prof. Şükrü Anıl Doğan sincerely, who challenged and constantly encouraged and supported me during this journey. I am honored to be part of your team and grateful for providing a research environment for all of us where we can brainstorm freely and share our crazy ideas. I could not have imagined a better mentor.

I would like to thank the members of my thesis jury members, Assoc. Prof. Aslı Kumbasar and Assoc. Prof. İbrahim Yaman for evaluating my thesis. I am very much looking forward to our discussion and hearing your constructive and challenging comments. Special thanks to İbrahim hocam for letting me use the qPCR machine repeatedly.

I am grateful to have Özlem Kartal and Mehmet Yılmaz as amazing lab mates who turned out to be great friends. I would like to extend my thanks to Bengi Bekmez, Sertan Atilla and Erdost Irmak for all their help in the crazy summer of 2022, I believe we learned a lot together.

My infinite thanks to my family and friends, whom I can also say are my chosen family, for always being there for me, always supportive, and always motivating, although even today, most of you, probably all of you, have no idea what I am doing in my academic life. My family, you have my endless gratitude and my love. Thank you, my mother, Yasemin Erkul, for always challenging and pushing me to do better; you made me the strong woman I am today. Thank you, my father, Mehmet Erkul, for always being there to catch me when I fall and believing in me even when I cannot. You are my all-time heroes. My brother, Bora Yağız Erkul, my partner in crime in driving mom and dad crazy, you are my absolute favorite person, and I cannot wait to jump into all the adventures awaiting us. My big family, all my uncles, aunts, and cousins, I do not even know how it is possible to have this cool and loving family. I love you all!

I know this is getting long but bear with me because I also know my friends will only read this section. To the gangs ‘Hepsi BIRAda’ and ‘4+1’, CHEERS! Thank you for all the crazy memories and unforgettable adventures, and laughter. Life is so enjoyable and fun with you. I missed you and hanging out with you incredibly!

This project was supported by the Scientific and Technological Research Council of Turkey (TÜBİTAK) research grant 321S547 to Şükrü Anıl Doğan. Semin Erkul has been supported by the TÜBİTAK-BİDEB 2210-A scholarship.

ABSTRACT

ALLEVIATING MITOCHONDRIAL MYOPATHY IN MICE

Mitochondrial dysfunction leads to a myriad of diseases, majority of which are caused due to respiratory chain (RC) deficiencies. Here, we demonstrate further molecular and morphological characterization of a skeletal muscle-specific mitochondrial Aspartyl-tRNA Synthetase (DARS2) knockout mouse model (mKO). The loss of DARS2 in skeletal muscle impaired mitochondrial translation, followed by RC deficiency, activation of adaptive stress responses, defective Complex IV (COX) activity, and reduced oxygen consumption rate. There is currently no cure for mitochondrial myopathy, but supportive methods have proven to be effective in alleviating the manifestation of the disorder. However, the effects of supportive treatments on early-onset mitochondrial myopathy cases and their relevant models remain to be discovered. Following characterization, we focused on the therapeutic effects of the Ketogenic Diet (KD) and 5-aminoimidazole-4-carboxamide ribonucleoside (AICAR) in mKO mice. The KD treatment partially rescued myopathy markers, such as recovery from mitochondrial integrated stress response (ISR^{mt}), increase in COX activity, and eliminated the blockage of autophagic flux without inducing mitochondrial biogenesis and prolonging the lifespan. The analysis of lipid metabolism revealed that DARS2-depleted skeletal muscle is highly dependent on glycolysis for energy production, and KD intervention caused the metabolism to shift further toward glucose utilization. AICAR treatment, on the other hand, induced muscle regeneration, recovery from ISR^{mt} and autophagic block; however, it further reduced COX activity and did not have an effect on mitochondrial biogenesis and lifespan. These findings extend our knowledge of the management of disease phenotypes of mitochondrial translation defects. Significantly, we proved that early-onset severe myopathy manifestation could not be sufficiently alleviated with treatments for mild late-onset myopathies, highlighting the importance of disease-specific treatments.

ÖZET

MİTOKONDRİYAL MİYOPATİ'NİN FAREDE İYİLEŞTİRİLMESİ

Solunum zinciri kusurlarının neden olduğu mitokondriyal bozukluklar geniş bir hastalık yelpazesini kapsar. Bu çalışmada, iskelet kasına özgü mitokondriyal aspartil-tRNA Sentetaz (DARS2) nakavt fare modelinin (mKO) moleküler ve morfolojik olarak ileri karakterizasyonu yapılmıştır. DARS2'nin iskelet kasındaki kaybı, mitokondriyal translasyonu bozmuş, ardından solunum zinciri yoksunluğuna, adaptif stres tepkilerinin aktivasyonuna, kusurlu Kompleks IV (COX) aktivitesi ve azalmış oksijen tüketimine neden olmuştur. Henüz mitokondriyal hastalıkların ilerlemesine engel olacak etkili bir tedavi yöntemi bulunamamıştır, ancak destekleyici yöntemlerin mitokondriyal miyopati belirtilerini hafifletmede etkili oldukları kanıtlanmıştır. Bununla birlikte, destekleyici tedavi yöntemlerinin erken ortaya çıkan mitokondriyal miyopati vakaları ve ilgili hastalık modelleri üzerindeki etkileri keşfedilmeyi beklemektedir. Bu çalışmanın ikinci bölümünde, nakavt farelerde Ketojenik Diyet (KD) ve 5-aminoimidazol-4-karboksamid ribonükleosit (AICAR) tedavi yöntemlerinin terapötik etkilerine odaklandık. KD tedavisi, mitokondriyal entegre stres yanıtında (ISR^{mt}) iyileşme gösterdi, artan COX aktivitesi dahil olmak üzere miyopati belirtilerini kısmen kurtardı ve mitokondriyal biyogenezi indüklemeden ve yaşam süresini uzatmadan otofajik akı üzerindeki tıkanıklığı ortadan kaldırdı. Lipit metabolizmasının analizi, DARS2'den yoksun iskelet kasının enerji üretimi için büyük ölçüde glikolize bağımlı olduğunu ve KD müdahalesinin metabolizmanın glikoz kullanımına daha fazla kaymasına neden olduğunu ortaya çıkardı. AICAR tedavisi ise kas rejenerasyonunu ve ISR^{mt} ve otofajik blokta iyileşmeyi indükledi; bununla birlikte, COX aktivitesini daha da azalttı ve mitokondriyal biyogenez ve yaşam süresi üzerinde ise bir etkisi olmadı. Bu bulgular, mitokondriyal translasyon kusurlarının hastalık fenotiplerinin yönetimi hakkındaki bilgimizi genişletmektedir. Önemli olarak, erken başlangıçlı şiddetli miyopati belirtileri, geç başlangıçlı hafif miyopatiler için uygulanan potansiyel tedavilerle yeterli seviyede hafifletilemez olduğunu gösterdik, bu da hastalığa özel tedavilerin önemini vurgulamaktadır.

TABLE OF CONTENTS

LIST OF FIGURES

LIST OF TABLES

LIST OF SYMBOLS

α	Alpha
&	And
β	Beta
◦C	Degree Celsius
γ	Gamma
gm	Gram
g	Gravity
kb	Kilo Base
m	Meter
μ	Micro
μg	Microgram
μl	Microliter
μM	MicroMolar
mg	Milligram
ml	Milliliter
mM	MiliMolar
min	Minute
M	Molar
nM	NanoMolar
pmol	Picomole
rpm	Revolution Per Volume
%	Percent
Ψ	Psi
s	Second
V	Volt

LIST OF ABBREVIATIONS

aaRS	Aminoacyl-tRNA Synthetases
AcoA	Acetyl coenzyme A
ADP	Adenosine Diphosphate
AICAR	5-Aminoimidazole-4-carboxamide-1-β-D-ribofuranoside
ATP	Adenosine Triphosphate
BSA	Bovine Serum Albumin
CCCP	Carbonyl Cyanide 3-Chlorophenylhydrazone
cDNA	Complementary DNA
COX	Cytochrome c Oxidase
Cre	Bacteriophage P1 derived site-specific recombinase
DARS2	Mitochondrial aspartyl-tRNA synthetase
ddH_2O	Double Distilled Water
DMSO	Dimethyl Sulfoxide
DNA	Deoxyribonucleic Acid
dNTP	Deoxyribonucleotide
ECL	Enhanced Chemiluminescence
ETC	Electron Transport Chain
FAD+	Flavin adenine dinucleotide
HCl	Hydrochloric Acid
H&E	Hematoxylin & Eosin Y
HRP	Horseradish Peroxide
H_2O_2	Hydrogen Peroxide
IBM2	Mitochondrial Isolation Buffer 2
IMB1	Mitochondrial Isolation Buffer 1

IMM	Inner mitochondrial Membrane
IMS	Intermembrane Space
ISR^{mt}	Mitochondrial Integrated Stress Response
KCl	Potassium Chloride
KD	Ketogenic Diet
K_2HPO_4	Potassium Hydrogen Phosphate
mAD	Modified Atkins Diet
$MgCl_2$	Magnesium Dichloride
mKO	Muscle-knockout
mRNA	Messenger RNA
mt-aaRS	Mitochondrial aminoacyl-tRNA Synthetases
mtDNA	Mitochondrial DNA
mt-tRNA	Mitochondrial tRNA
NaCl	Sodium Chloride
NaF	Sodium Fluoride
NAD+	Nicotinamide adenine dinucleotide
NBT	Nitro Blue Tetrazolium
OMM	Outer Mitochondrial Membrane
PCR	Polymerase Chain Reaction
PBS	Phosphate Buffered Saline
PMS	Phenylmethanesulfonyl fluoride
pH	Potential of Hydrogen
qPCR	Real-Time PCR
RNA	Ribonucleic Acid
ROS	Reactive Oxygen Species
SDH	Succinate dehydrogenase
SDS	Sodium Dodecyl Sulfate

SEM	Standard Error of Mean
TEMED	Tetramethyl Ethylenediamine
Tris	2-Amino-2-(Hydroxymethyl)-1,3-Propandiole
Tris HCl	2-Amino-2-Hydroxymethyl-Propane-1,3-Diol
tRNA	Transfer RNA
TWEEN	Polyoxyethylene-Sorbitan-Monolaureate
WT	Wild Type

1. INTRODUCTION

1.1. Mitochondria: Powerplants of the Cell

The widely accepted endosymbiotic theory states that the mitochondrion was once a free-living organism, an α-proteobacterium that was engulfed by a eukaryotic host cell millions of years ago. Rather than being digested by the host cell, the two organisms started a symbiotic relationship, the host cell providing a safe place for the bacterium in return for cellular energy produced by the organelle, and in time they evolved together to form complex living organisms as we know of today (Margulis, 1970). This theory was based on the evidence of the free-living past of the organelle. Just like bacteria, mitochondria contain their own circular DNA, mitochondrial DNA (mtDNA), along with transcription and translation systems. However, during the process of evolution, mtDNA significantly reduced in size, perhaps by transferring its genes to the nucleus to protect from mutations and expand their expression (Shutt & Gray, 2006; Lane & Martin, 2010).

This theory is further supported by the formation of dynamic mitochondrial networks through fission and fusion, mimicking prokaryote proliferation. The constant remodeling of the network allows the cell to adapt to metabolic changes and respond to stress (Pernas & Scorrano, 2016; Wai & Langer, 2016). As double-membraned organelles, mitochondria consist of an outer mitochondrial membrane (OMM) and an inner mitochondrial membrane (IMM). The space that separates the OMM and the IMM is termed the intermembrane space. Like eukaryotic cell membranes, the OMM is permeable to small molecules, whereas the IMM is less permeable and contains cardiolipin, similar to prokaryotic membranes (Zalman et al., 1980; Protasoni & Zeviani, 2021). The cristae are formed through the invagination of the IMM toward the matrix, hosting the Respiratory Chain (RC) complexes. The metabolic processes, including Tricarboxylic Acid (TCA) Cycle and β-oxidation, occur in the matrix, where mitochondrial transcription and translation occur (Frey & Mannella, 2000).

The mtDNA is packed with nucleoids in the matrix, which contains a light (9 genes) and a GC-rich heavy strand (28 genes), encoding 37 genes, 13 RC subunits, 22 transfer RNAs (tRNAs), and 2 ribosomal RNAs (rRNAs) (Anderson et al., 1981). Unlike the nuclear genome, the mitochondrial genome is devoid of introns, but instead contains a non-coding region named displacement loop (D-loop), where the transcriptional and translational promoters reside (Falkenberg, 2018). The human mtDNA is 16,569 base pairs, and depending on the cell type, a single human cell can contain around 100 to 1000 mtDNA (Anderson et al., 1981; Spelbrink et al., 2001). In cases of mutations on the mitochondrial genome, cells can either be homoplasmic (containing identical mtDNAs) or heteroplasmic (containing multiple versions of mtDNA). The mtDNA is maternally inherited with oocytes, and if the oocyte is heteroplasmic, the baby can also inherit the heteroplasmy. The mutation on the mitochondrial genome can lead to mitochondrial diseases/defects depending on the amount of mutated mtDNA exceeding the threshold (Birky, 2001; Rawi et al., 2011).

Mitochondria are best known for their function as predominant energy producers by oxidative degradation of nutrients (carbohydrates, amino acids, and fatty acids) into adenosine triphosphate (ATP) (Mitchell, 1961). To be involved in the process of ATP synthesis through oxidative phosphorylation (OXPHOS), nutrients first need to be converted into Acetyl-coenzyme A (Acetyl-CoA). In the cytoplasm, amino acids are deaminated and metabolized to pyruvate or tricarboxylic acid cycle (TCA cycle) intermediates, and through glycolysis, glucose is broken down into 2 molecules of ATP, NADH, and pyruvate, are then transferred to mitochondria and converted into Acetyl-CoA. On the other hand, fatty acids are transferred to mitochondria through the carnitine shuttle system to produce Acetyl-CoA with mitochondrial β-oxidation in the matrix. NADH and $FADH_2$ cofactors produced during the process can also be fed to the respiratory chain (RC) (Nelson & Cox, 2017). β-oxidation is the major energy source for high energy-consuming organelles, including the brain (Goldstein et al. 1953), cardiac (Ballard et al. 1960), and resting state skeletal muscle tissues (Dagenais et al., 1976). During exercise, skeletal muscle mostly depends on glucose energy production (Goldstein et al., 1953).

As the first step of the TCA cycle, oxaloacetate reacts with Acetyl-CoA, which is followed by a series of reactions, generating electron carriers by reducing NAD^+ and FAD^+

into NADH and $FADH_2$ and regenerating oxaloacetate as the name TCA cycle suggests. Besides its central role in energy production, the TCA cycle also provides intermediates for the biosynthesis of nucleotides (Nunnari & Suomalainen, 2012).

The reduced cofactors NADH and $FADH_2$, generated from β-oxidation and TCA cycle, are donated to the RC. Among many important cellular reactions harbored by mitochondria, OXPHOS is one of the most critical functions which provides the majority of cellular energy (Mitchell, 1961). The OXPHOS system is catalyzed by four multi-subunit complexes, constituting the electron transport chain (ETC) and an F_0F_1 ATP synthase (Complex V), all embedded in the mitochondrial inner membrane (Pereira, 2020). NADH and $FADH_2$ are oxidized by a NADH dehydrogenase (Complex I) and succinate dehydrogenase (Complex II), respectively, and the electrons are transferred to ubiquinone across ubiquinol-cytochrome c oxidoreductase (Complex III) and cytochrome c oxidase (Complex IV) (Nolfi-Donegan et al., 2020). Complex I, III, and IV utilize energy to pump protons across the inner membrane into the intermembrane space, generating a potential, but only the latter reduces oxygen into two water molecules. Complex V uses the generated electrical and chemical proton gradient to carry those protons back to the matrix and drive the phosphorylation of adenosine diphosphate (ADP) to ATP (Mitchell, 1961; Mitchell & Moyle, 1967).

CI is the largest among RC complexes and consists of 45 subunits, forming 2 domains; matrix and membrane are both containing 7 core subunits. The matrix arm harbors NDUFS1, NDUFS2, NDUFS3, NDUFS7, NDUFS8, NDUFV1, and NDUFV2 along with flavin mononucleotide (FMN) and a final electron accepting FeS cluster (N2 cluster). The membrane arm contains seven hydrophobic subunits encoded by the mitochondrial genome, ND1-6 and NDUL (Sharma et al. 2009; Carroll et al., 2006). The second entry point for the electrons to the RC is Complex II through TCA cycle intermediate succinate, serving as the link between the metabolism and OXPHOS. CII consists of four nuclear-encoded subunits: two matrix-located subunits (SDHA and SDHB), containing a binding site for the succinate, and two hydrophobic membrane-anchor subunits (SDHC and SDHD), containing a ubiquinone binding site (Bezawork-Geleta et al., 2017). Complex III is a symmetrical dimer containing 11 subunits per monomer and transfers electrons from ubiquinone to cytochrome

c, pumping two protons to intermembrane space. CIV has thirteen subunits with 3 core subunits encoded in the mitochondrial genome and ten nuclear-encoded accessory subunits. CIV donates electrons from cytochrome c to the terminal electron acceptor oxygen and produces water while pumping four protons to intermembrane space (Li et al., 2021). The proton gradient generated by the ETC is used for energy production by CV, which consists of an inner mitochondrial membrane element F_0 domain as the proton channel and a catalytic F_1 domain located in the matrix (Chaban et al., 2014; Sousa et al., 2018). Energy production by OXPHOS is highly efficient by generating 36 ATP on average per glucose molecule (Nelson & Cox, 2017).

Energy production is not the only function of mitochondria. In addition, mitochondria play an essential role in cell homeostasis, participating in the biosynthesis of amino acids, lipids, heme, and iron-sulfur clusters, regulation of intra- and intercellular signaling, and reactive oxygen species (ROS) production.

1.2. Regulation of Mitochondrial Translation

The synthesis and import of nuclear-encoded proteins to mitochondria, besides mitochondrial DNA-encoded protein synthesis, are required for the assembly of RC (Pereira, 2020). These proteins are imported to the mitochondria by the outer membrane (Translocase of the Outer Membrane, TOM and beta-barrel-specific Sorting and Assembly Machinery, SAM) and inner mitochondrial membrane (Translocase of the Inner Membrane, TIM) proteins (Neupert & Hermann, 2007).

All 22 tRNAs, encoded in the mitochondrial genome, are needed to translate 13 mtDNA-encoded RC proteins. For this reason, these tRNAs should be charged with their cognate amino acids, a process called “tRNA charging.” In eukaryotic cells, the nuclear genome encodes for two sets of aminoacyl-tRNA synthetases (aaRSs); both work for the same task but in different compartments of the cell cytoplasm and mitochondria. The catalytic site of aaRS hydrolyses ATP into AMP and pyrophosphate (PPi) and attaches AMP to the amino acid, while PPi is released. Then, the AMP-attached amino acid is transferred

to the corresponding tRNA. Following this, the vacant AMP and charged tRNA are released from the aaRS Figure 1.1 (Konovalova & Tyynismaa, 2013; Kaiser et al., 2020).

Mt-aaRSs are essential for mitochondrial protein synthesis; mutations affecting their function can give rise to a wide range of mitochondrial diseases. For example, mutations in the mitochondrial aspartyl-tRNA synthetase (*DARS2*) gene, which encodes the protein that attaches aspartate to its cognate tRNA in mitochondria, cause Leukoencephalopathy with Brainstem and Spinal cord involvement of high Lactate (LBSL) (Scheper et al., 2007). The disorder is inherited in an autosomal recessive manner, slowly developing progressive spasticity, cerebellar ataxia, and deterioration of motor skills. A common frameshift mutation in patients is located on the splice site of intron 2, upstream of exon 3, forming a non-functional protein. However, in some cases, full-length functional DARS2 has been detected in patients. There has not been a cure for LBSL, and until today, treatments are directed toward the symptoms, which can differ in different patients and be observed at any age (van Berge et al., 2012).

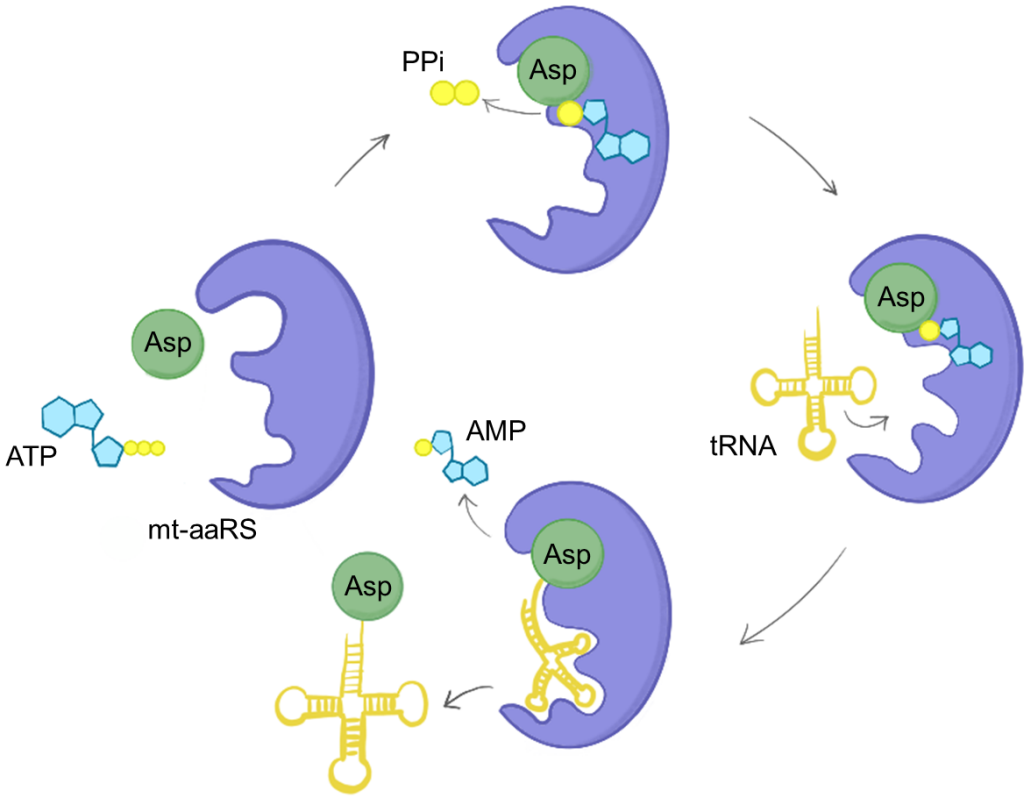

Figure 1.1. tRNA charging with aspartate in mitochondria.

1.3. Mitochondrial Dysfunction and Stress

Mitochondrial disorders are mostly defined as clinical syndromes caused by defects in OXPHOS and are the most common errors in our metabolism. These disorders are clinically and genetically heterogenous and are the only genetic condition in humans that has the involvement of two genomes, mitochondrial and nuclear (Dogan et al., 2014). Because of the complex pathology of the disorders, any organ can be affected and the disease can be observed at any age. Currently, no cure is available; the management methods are limited to palliative measures against symptoms and progression, most of which are focused on increasing mitochondrial biogenesis and function (Davison & Rahman, 2017). One of the significant challenges in developing curative treatments is obtaining samples from a homogenous cohort of patients, which makes mouse studies critically crucial for treatment development (Pfeffer et al., 2011). A subset of mitochondrial disorders is mitochondrial myopathy, the primary prognosis of prominent muscular dysfunction. The most common characteristic observed in mitochondrial myopathy patients is muscle weakness, atrophy, histological changes in muscle tissue, and exercise intolerance, which are strongly observed in the model developed previously by our lab (Pfeffer & Chinnery, 2013).

1.3.1. Mitochondrial Biogenesis

Mitochondrial mass and function are balanced by mitochondrial biogenesis and turnover (mitophagy), which greatly varies in different cell types and tissues (Lehman et al., 2000). A complex of transcription factors and cofactors regulate mitochondrial biogenesis, such as Nuclear Respiratory Factors 1 and 2 (NRF1 and NRF2) and peroxisome Proliferator-activated receptor Gamma Cofactor α (PGC1α) (Scarpulla et al., 2012).

PGC1α regulates cellular energy metabolism by interacting with a wide range of transcription factors, including NRF1 and NRF2, involved in various biological responses, such as mitochondrial biogenesis and β-oxidation (Gureev & Popov, 2019; Liang & Ward, 2006). Induction of mitochondrial biogenesis through PGC1α overexpression has been shown to alleviate mitochondrial defects in mouse models (Viscomi et al., 2011). PGC1α

interacts with α, β/δ, and γ isoforms of the peroxisomal proliferator-activated receptors (PPARs). PPARs are ubiquitously expressed in different tissues and are involved in the regulation of genes associated with mitochondrial and peroxisomal fatty acid uptake and β-oxidation (Lefebvre et al. 2006). PGC1α can be activated via direct phosphorylation by the AMP-activated protein kinase (AMPK) or through deacetylation by NAD^+-dependent sirtuin 1, Sirt1. AMPK is activated through phosphorylation when the cellular AMP levels are higher than ATP, highlighting the need for energy in the cell. As a consequence of AMPK activation, energy-producing processes are induced, including OXPHOS and β-oxidation, whereas the energy-consuming activities are halted (Cantó & Auwerx 2010).

NRF1 and NRF2 regulate the expression of RC subunits, encoded by nuclear DNA and involved in mtDNA transcription. NRF1, but not NRF2, induces the expression of TFAM (transcription factor A, mitochondrial), which is required for the maintenance of mtDNA and in direct relation with its replication. Translocation of NRF2 to the nucleus is conducted by an activated form of AMPK (Gureev & Popov, 2019).

1.3.2. Mitochondrial Integrated Stress Response (ISR^{mt})

A hallmark of mitochondrial dysfunction is the induction of mitochondrial integrated stress response (ISR^{mt}), which can be triggered by unfolded protein stress and nutrient deficiency (Dogan et al., 2014). The name comes from the combination of the response targets, unfolded protein response transcripts, metabolites, and redox signaling (Suomalainen & Battersby, 2018). As a response to such stimuli and mitochondrial dysfunction, the alpha subunit of translation initiation factor 2 (eIF2α) is phosphorylated, which causes the inhibition of cytoplasmic protein synthesis but induces the translation of transcription factors, such as ATF4, ATF5, and CHOP, promoting metabolic rewiring along with the synthesis of amino acids and antioxidants (Mick et al., 2020).

The mitochondrial folate cycle, a part of one-carbon metabolism providing formyl-methionine that is used in initiating mitochondrial translation, is induced by cell-autonomous ISR^{mt}. The methylenetetrahydrofolate dehydrogenase 2 (MTHFD2) regulates the

mitochondrial folate cycle and is only induced during times of stress. PYCR1 protein levels are elevated to induce proline synthesis due to its depletion in mitochondrial deficiencies (Licari et al., 2021). The ISR^{mt} can also induce fibroblast growth factor 21 (FGF21) and growth differentiation factor 15 (GDF15) expression as a secretory signal and remodel energy metabolism for the entire organism (Suomalainen & Battersby, 2018).

1.3.3. Autophagy

Autophagy is a conserved degradation process of the cell, in which unfunctional organelles, and aggregated or misfolded proteins are eliminated as a survival mechanism to preserve cell homeostasis (Glick et al., 2010). The damaged or nonfunctional mitochondria are engulfed by autophagosomes and degraded by lysosomes to optimize the state of a "healthy" mitochondria population. Protein quality in the nucleus and cytoplasm is controlled by the protein P62, which delivers ubiquitinated proteins to autophagosomes and facilitates autophagic degradation by binding LC3-II. The level of P62 and the conversion of cytosolic-free LC3-I to autophagosome-associated LC3-II by lipidation have been used as a reporter of autophagy activity; a decrease in both P62 level and LC3-II/LC3-I ratio is associated with an increase in autophagy due to the degradation of P62 and LC3II during the process (Giménez-Xavier et al., 2008; Liu et al., 2016; Dogan et al., 2014).

1.4. Mitochondrial Translational Deficiency Mouse Models

The whole-body knockout mouse models discussed next had impaired mitochondrial translation and died in embryonic stages, except the mouse models with *Pus1* and *Wars2* deficiency, yet tissue-specific conditional ablation of the genes led to premature death, signifying the importance of mitochondrial protein homeostasis in development and aging. The studies on the mouse models provide valuable insights into understanding how tissues develop metabolic adaptive responses against mitochondrial translation deficiency (Metodiev et al., 2009; Cámara et al., 2014; Mourier et al., 2014; Dogan et al., 2014; Iommarini et al., 2015).

The mitochondrial transcription factor B1, *Tfb1m*, is involved in mitochondrial translation through the activity of rRNA methyltransferase. Heart and skeletal muscle-specific *Tfb1m* KO mouse model developed severe cardiomyopathy and impaired RC function with increased mitochondrial cardiomyopathy, while the skeletal muscle remained unaffected by mitochondrial abnormalities (Metodiev et al., 2009; Iommarini et al., 2015).

MTERF4, mitochondrial termination factor 4, is directly involved in mitochondrial translation and crucial for ribosomal assembly, and its heart and skeletal muscle-specific depletion manifested cardiomyopathy in the mouse model. *Mterf4* KO mice showed reduced RC complex assembly and induced mitochondrial biogenesis (Cámara et al., 2014; Iommarini et al., 2015).

Leucine-rich pentatricopeptide repeat-containing protein, LRPPRC, is a mitochondrial matrix protein that participates in mitochondrial protein translation and stability. Heart and skeletal muscle *Lrpprc* KO mice elicited CIV deficiency and developed cardiomyopathy. In contrast, heart-specific KO of *Lrpprc* revealed a defect in the CV assembly with increased ROS levels and mitochondrial potential (Mourier et al., 2014; Iommarini et al., 2015).

Heart and skeletal muscle *Dars2* KO mice showed RC deficiency due to impaired mitochondrial protein synthesis. In the heart, DARS2 depletion induced mitochondrial biogenesis and mitochondrial unfolded protein response along with upregulation of *Fgf21*, whereas downregulated autophagy. On the other hand, skeletal muscle tissue was resistant to perturbed protein homeostasis and did not exhibit the responses observed in the heart, highlighting that different tissues can react and adapt differently to the same conditional changes (Dogan et al., 2014; Iommarini et al., 2015).

The mouse model of mitochondrial myopathy with lactic acidosis and sideroblastic anemia lacks pseudouridine modifications in cytoplasmic and mitochondrial tRNAs due to *Pus1* deletion, resulting in a shortened lifespan of 14 weeks. The mouse model displayed

reduced Succinate dehydrogenase (SDH) and Cytochrome c oxidase (COX) activity accompanied by decreased exercise capacity (Magnum et al., 2016).

A mutant mouse model for the mitochondrial tryptophanyl-tRNA synthetase 2 (Wars2) gene developed progressive tissue-specific pathologies, such as cardiomyopathy, adipose tissue dysfunction, and hearing loss, highlighting the activation of ISR by different mechanisms that might be important for tissue specificity (Agnew et al., 2018).

A skeletal muscle-specific mitochondrial translation deficient mouse model was generated in a previous project studied in our lab, discussed in detail in 5.1-5.4.

1.5. Interventions for Mitochondrial Myopathy

Besides the disorders caused by primary mitochondrial dysfunction, there are diseases involved intensely with mitochondria, including diabetes, cancer, Parkinson and what we are all facing; aging, drawing the interest in therapeutic research (Nunnari & Suomalainen, 2012). Despite the challenges of heterogeneity and the complexity of the disorders, studies on alleviating disease symptoms in laboratory animals have been crucial in developing new treatment methods.

1.5.1. Ketogenic Diet

Mitochondrial disease patients with inadequate diets develop worsening disease symptoms. It is essential for patients to have an adequate healthy diet and avoid fasting (Zweers et al., 2017). A low carbohydrate, high fat ketogenic diet has been proposed as a therapy for children with epilepsy and a possible treatment for mitochondrial diseases patients with RC deficiency and Alpers syndrome (Kang et al., 2007; Joshi et al., 2009). The diet's high lipid content stimulates the metabolism shift from glycolysis to mitochondrial β-oxidation. As mitochondria are left as the only energy-producing compartment in the cell

due to lack of glucose, an increase in the transcription of genes associated with the TCA cycle and OXPHOS has been observed in hippocampal neurons (Bough et al., 2006). The transgenic Deletor mice, a late-onset mitochondrial myopathy model overexpressing mtDNA helicase Twinkle, which causes accumulation of mtDNA deletions, under KD treatment showed decelerated disease progression. The study revealed the positive effects of diet intervention on reducing the number COX-negative fibers and rescuing the muscle from the formation of mitochondrial abnormalities, in addition to activation of mitochondrial biogenesis and recovery from metabolic alterations observed in the mouse model (Ahola-Erkkilä et al., 2010). As a consequence of the promising results from mouse model studies, the researchers wanted to utilize KD treatment in patients. The ketogenic diet "modified Atkins diet" (mAD) study on progressive external ophthalmoplegia (PEO) patients with mitochondrial myopathy revealed that dietary changes could modify disease progression. During the study, five patients had acute muscle pain after 1-2 weeks due to diet changes, and the study was terminated. However, the diet caused damage, especially to the ragged red fibers, a hallmark of mitochondrial myopathy. In long-term follow-up, improvement in muscle strength and regeneration was observed in patients. As diet plays a significant role in disease progression, dietary counseling should be part of treatments for mitochondrial myopathies (Ahola et al., 2016).

1.5.2. 5-aminoimidazole-4-carboxamide ribonucleoside (AICAR)

The pharmacological compound AICAR can induce PGC1α activation via AMPK, previously discussed in 1.3.1 Mitochondrial Biogenesis. AICAR generates inosine monophosphate, mimics AMP, and therefore activates AMPK in a similar fashion to AMP/ATP ratio (Merrill et al., 1997; Viscomi et al., 2011). In skeletal muscle, activated AMPK regulates various metabolic processes, including mitochondrial biogenesis, β-oxidation, glucose uptake, and glycogen synthesis. It has been shown that AICAR treatments in a dosage-dependent manner can increase RC activity, mitochondrial mass (mitochondrial biogenesis), motor performance, and memory function in several mouse models (Viscomi et al., 2011; Jahnke et al., 2012; Peralta et al., 2016; Kobilo et al., 2014). In skeletal muscle samples of type 2 diabetes patients, AICAR treatment increased glucose uptake (Koistinen et al., 2003).

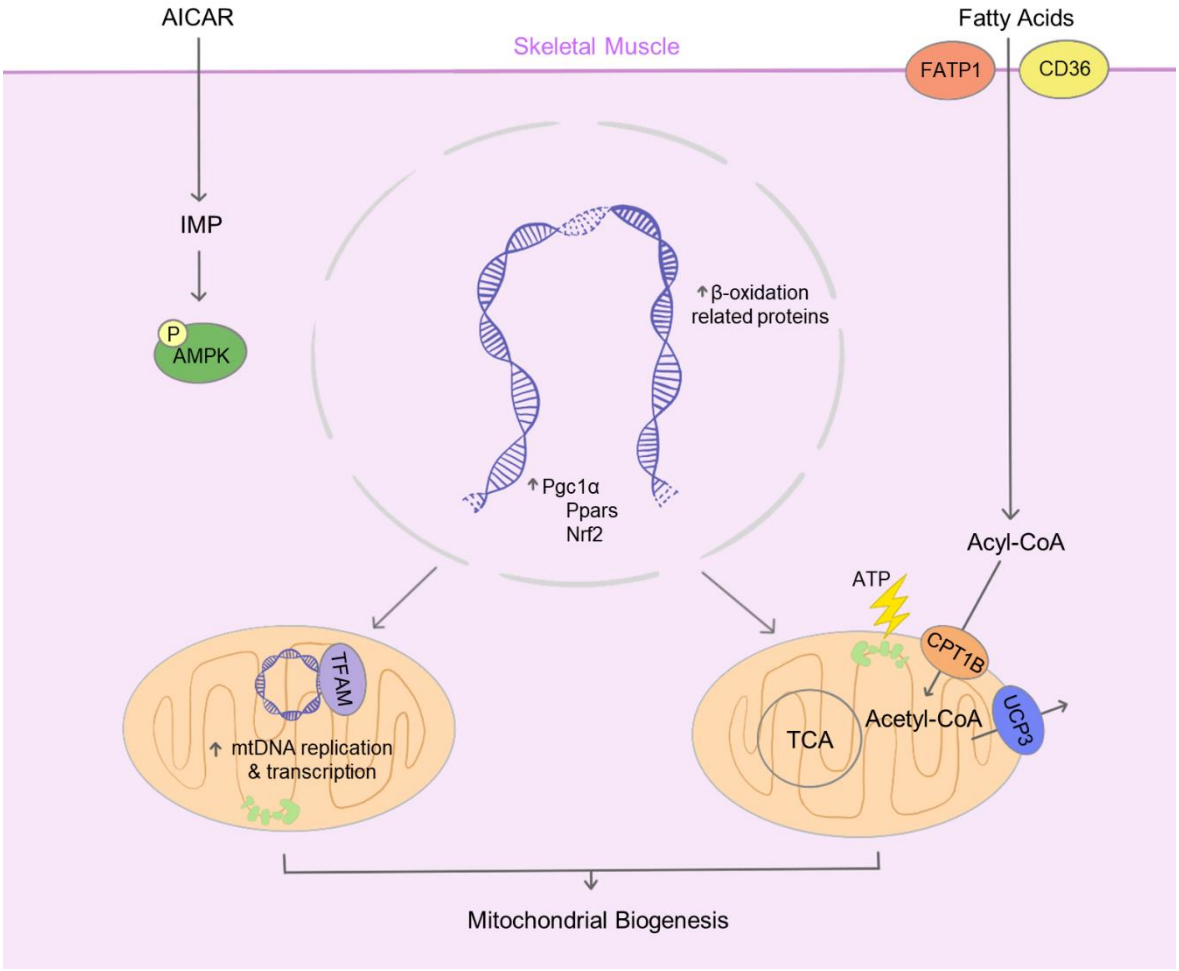

Figure 1.2. The representative presentation of the effects of KD and AICAR on molecular mechanisms in skeletal muscle cells.

2. PURPOSE OF THE STUDY

The overall objective of this study is to evaluate the impact of potential therapeutic methods on alleviating symptoms of mitochondrial myopathy. The specific aims are as follows,

- To further characterize the skeletal muscle-specific DARS2 KO mouse model (mKO) through histology and molecular biology.
- To alleviate the consequences of tissue-specific DARS2 depletion by ketogenic diet intervention.
- To attenuate the effects of skeletal muscle-specific DARS2 depletion by daily 5-aminoimidazole-4-carboxamide ribonucleoside (AICAR) injection.

3. MATERIALS

3.1. Antibody List

Antibodies used in this study are given in table 3.1.

Table 3.1. Antibody List.

Antibody	Supplier	Catalog Number
Anti-Mouse HRP-linked	Cell Signaling Technologies	7076S
Anti-Rabbit HRP-linked	Cell Signaling Technologies	7074S
AMPKa	Cell Signaling Technologies	2532S
eIF2-α	Cell Signaling Technologies	9722
HSC 70	Santa Cruz Biotechnology	D0318
Hsp60	Abcam	ab46798
LC3B	Cell Signaling Technologies	2775S
NRF2	Cell Signaling Technologies	12721S
Total OXPHOS Blue Native WB Cocktail	Abcam	ab110412
PGC-1α	Santa Cruz Biotechnology	sc-518025
Phospho-AMPKa	Cell Signaling Technologies	2531S
Phospho-eIF2-α	Cell Signaling Technologies	3398

Table 3.1. Antibody List. (cont.)

Antibody	Supplier	Catalog Number
PYCR1	Proteintech	13108-1-AP
SOD2	Cell Signaling Technologies	13141S
TFAM	Abcam	ab131607
VDAC1/Porin	Proteintech	55259-1-AP

3.2. Buffers and Solutions

Buffers and solutions for the experiments in this thesis are listed in table 3.2.

Table 3.2. Buffers and Solutions.

Buffers & Solutions	Content
DNA Extraction Buffer	200 mM NaCl
	10 mM Tris-HCl (pH: 8)
	5 mM EDTA (pH: 8)
	0.2% SDS
Mitochondria Isolation Buffer 1 (pH: 7.4)	67 mM Sucrose
	50 mM KCl
	50 mM Tris-HCl
	10 mM EDTA
	0.2% BSA (Fatty acid-free)
Mitochondria Isolation Buffer 2 (pH: 7.4)	250 mM Sucrose
	0.3 mM EGTA-Tris
	10 mM Tris-HCl

Table 3.2. Buffers and Solutions. (cont.)

Buffers & Solutions	**Content**
Organ Lysis Buffer	50 mM HEPES (pH: 7.4)
	1% Triton X-100
	2.3 M NaF
	10 mM Na-Orthovanadate
	10 mM EDTA
	0.1% 20X SDS
	50 mM NaCl
10X PBS	100 mM Na_2HPO_4
	1.8 mM KH_2PO_4
	1.37 M NaCl
	27 mM KCl
1X PBS-T	100 ml 10X PBS
	900ml ddH2O
	0.1% Tween-20
10X Running Buffer	25 mM Tris
	250 mM Glycine
	0.2% SDS
10% Resolving Gel	3.94 mL ddH2O
	2 mL Tris (pH:8.8 & 1.5M)
	1.98 mL 40% Acrylamide
	80 µL 10% SDS
	8 µL TEMED
	80 µL 10% APS
5% Stacking Gel	2.45 mL ddH2O
	1 mL Tris (pH:6.8 & 1M)
	487.5 µL 40% Acrylamide
	40 µL 10% SDS
	4 µL TEMED
	20 µL 10% APS

Table 3.2. Buffers and Solutions. (cont.)

Buffers & Solutions	Content
10X Transfer Buffer	250 mM Tris
	1.92M Glycine
1X Transfer Buffer	100 ml 10X Transfer Buffer
	200 ml Absolute Methanol
	700 ml ddH2O

3.3. Chemicals

The chemicals used in this study are given in table 3.3.

Table 3.3. Chemicals.

Chemicals	Supplier
Acetic Acid (Glacial) 100% Anhydrous	Isolab, Germany
Acetyl coenzyme A Lithium Salt	Sigma-Aldrich, USA
Acrylamide-Bisacrylamide 40%	Neofroxx, Germany
Adenosine 5′-diphosphate monopotassium salt dihydrate	Sigma-Aldrich, USA
Agarose	GeneOn, Germany
5-Aminoimidazole-4-carboxamide-1-β-D-ribofuranoside (AICAR)	TRC, Canada
Ammonium Acetate	Merck, Germany
Ammonium persulfate	Biofroxx, Germany
AmplexTM Red Reagent	Sigma-Aldrich, USA
Antimycin A	Sigma-Aldrich, USA
Boric Acid	Merck, Germany
BSA	Neofroxx, Germany
BSA (fatty acid-free)	Sigma-Aldrich, USA
CCCP	Sigma-Aldrich, USA

Table 3.3. Chemicals. (Cont.)

Chemicals	Supplier
Coomassie Brilliant Blue R250	Neofroxx, Germany
Cytochrome C from bovine heart	Sigma-Aldrich, USA
Diaminobenzidine tetrahydrochloride	Sigma-Aldrich, USA
Dimethyl Sulfoxide (DMSO) for molecular biology	Neofroxx, Germany
di-Potassium hydrogen phosphate anhydrous	Merck, Germany
di-Sodium hydrogen phosphate	Merck, Germany
DPX	Thermo Fisher, USA
EDTA	Biofroxx, Germany
EGTA	Biofroxx, Germany
Eosin Y-solution 0.5% aqueous	Merck, Germany
Ethanol Absolute≥ 99.9%	Isolab, Germany
Ethanol Absolute For Analysis 2.5Lt	Merck, Germany
Ethidium Bromide	Neofroxx, Germany
GeneRuler 1kb DNA ladder	Thermo Fisher, USAhor
Glycine	Neofroxx, Germany
HEPES buffer	Biofroxx, Germany
Hematoxylin solution modified acc. To Gill III	Merck, Germany
Horseradish peroxidase	Sigma-Aldrich, USA
Hydrogen Peroxide	Merck, Germany
Ketogenic Diet	Optima, Turkey
K2HPO4	Merck, Germany
Methanol ≥ 99.8%	Isolab, Germany
Milk Powder	Havancızade, Turkey
Nitro Blue Tetrazolium	Sigma-Aldrich, USA
NuPAGE LDS Sample Buffer (4X)	Invitrogen, USA
NuPAGE Sample Reducing Agent	Invitrogen, USA

Table 3.3 Chemicals. (cont.)

Chemicals	Supplier
Oligomycin A	Sigma-Aldrich, USA
PageRuler Plus Prestained Protein Ladder	Thermo Fisher, USA
PageRuler™ Protein Ladder, 10 to 180 kDa	Thermo Fisher, USA
Phenylmethanesulfonyl fluoride	Sigma-Aldrich, USA
2-Propanol	Merck, Germany
Ponceau S	Ecotech, Turkey
Potassium chloride	Merck, Germany
Potassium hydroxide	Sigma-Aldrich, USA
Proteinase K	Biofroxx, Germany
Rotenone	Sigma-Aldrich, USA
Safranin O	Sigma-Aldrich, USA
Saline (0.9% Isotonic Sodium Chloride)	Polifarma, Turkey
SDS	Biofroxx, Germany
Sodium Acetate	Merck, Germany
Sodium Chloride	Merck, Germany
Sodium Floride	Neofroxx, Germany
Sodium Hydroxide	Merck, Germany
Sodium Orthovanadate	Sigma-Aldrich, USA
Sodium phosphate dibasic dihydrate	Sigma-Aldrich, USA
Sodium pyruvate	Sigma-Aldrich, USA
Sodium Succinate dibasic hexahydrate	Sigma-Aldrich, USA
Sucrose	Caisson Labs, USA
TEMED	Neofroxx, Germany
TES	PanReac AppliChem, USA
Trypsin-EDTA (0.5%)	Thermo Fisher, USA
Tissue-Tek ® O.C.T. ™ Compound	Sakura, USA
Tris-HCl	Promega, USA
Triton X-100	Biofroxx, Germany

Table 3.3. Chemicals (cont.)

Chemicals	Supplier
TWEEN20	Neofroxx, Germany

3.4. Kits and Enzymes

The kits and enzymes used in this study are given in table 3.4.

Table 3.4. Kits and Enzymes

Kits & Enzymes	Supplier
DC Protein Assay Kit	Bio-Rad, USA
GoTaq G2 DNA Polymerase	Promega, USA
iScriptTM cDNA Synthesis Kit	Bio-Rad, USA
RealQ Plus 2x Master Mix Green	Ampliqon, Denmark
WesternBright ECL – HRP Substrate	Advansta, USA
WesternBright Sirius Chemiluminescent Detection Kit	Advansta, USA
Zymo Research Directzol RNA MiniPrepPlus	Zymo Research, USA

3.5. Laboratory Equipment and Devices

The laboratory equipments and devices used in this study are given in table 3.5.

Table 3.5. Laboratory Equipments and Devices

Equipment or Devices	Supplier
$+4^0$C Room	Birikim Elektrik Sogutma, Turkey
$+37^0$C Room	Birikim Elektrik Sogutma, Turkey

Table 3.5. Laboratory Equipment and Devices (cont.)

Equipment or Devices	Supplier
Accu-Check Glucometer	Roche, Switzerland
Accu-Check Glucometer Strips	Roche, Switzerland
Activity Cage	Ugo Basile, Italy
Agarose Gel Electrophoresis System	Analytic Jena, Germany
Autoclaves	Astell, UK
Biometra TSC ThermoShaker	Analytik Jena, Germany
Centrifuge	Hitachi Koki, Japan
Coverslips	Marienfeld, Germany
Cryomold® Molds/Adapters	Tissue-Tek, USA
Cryopure Tubes	Sarstedt, Germany
Cryostat CM3050	Leica Microsystems, US
Deep freezer (-20)	Arçelik, Turkey
Deep freezer (-80)	Thermo, UK
Dish Washer	Mielabor G7783, Miele, Germany
Falcon Tubes	Sarstedt, Germany
G-BOX Chemi XX6	Syngene, UK
Gel Doc XR System	Bio-Doc, Italy
Glass Bottles	Isolab, Germany
Grip Strength Meter	Ugo Basile, Italy
Heat Blocks	Analytic Jena, Germany
Ice Maker	Scotsman Inc. AF20, Italy
Magnetic Fish	Isolab, Germany
Magnetic Stirrer	Chiltren, USA
Microscope slides- Superfrost plus	Thermo Fisher Scientific, USA
Micropipettes	Axygen, USA
Micropipette Tips	Axygen, USA
Microtome Blades	Thermo Fisher Scientific, USA
Microwave Oven	Arcelik, Turkey
Multiwell Plates	Topscien, China

Table 3.5. Laboratory Equipments and Devices. (cont.)

Equipment or Devices	Supplier
Nitrocelluluse Blotting Membrane	Amersham, UK
O2k-FluoRespirometer	Oroboros Instruments, Austria
PCR Machine	Biorad, USA
PCR Tubes	Axygen, USA
Petri Dishes	Fırat Plastik, Turkey
pH Meter	Hanna Instruments, USA
Pipettor	Axygen, USA
Plate Reader	VersaMax, Molecular Devices, USA
Power Supply	Biorad, USA
Refrigerators	Bosch, Germany
Rotarod	Ugo Basile, Italy
Rotator	Onilab, USA
QPCR Machine	Bioneer Exicycler, Republic of Korea
SDS-PAGE Transfer System	Biorad, USA
Serological Pipettes	Sarstedt, Germany
Shakers	Onilab, USA
Spectrophotometer	Nanodrop ND-100 Thermo, USA
Super PAP Pen	Isolab, Germany
Syringes	Set inject, Turkey
Treadmill	Ugo Basile, Italy
Vortex	IKA, USA
Water distillator	UTES, Turkey
Watmann Filter Paper-Extra Thick	Thermo Fisher, USA

3.6. Primers

The primers used in this study are given in table 3.6.

Table 3.6. Primer List

Primer Name	Sequence (5'-3')
Catalase_F	TGGCACACTTTGACAGAGAGC
Catalase_R	CCTTTGCCTTGGAGTATCTGG
Cd36_F	TGCTGGAGCTGTTATTGGTG
Cd36_R	TGGGTTTTGCACATCAAAGA
Cpt1b_F	TCGCAGGAGAAAACACCATGT
Cpt1b_R	AACAGTGCTTGGCGGATGTG
Chop_F	CTGGAAGCCTGGTATGAGGAT
Chop_R	CAGGGTCAAGAGTAGTGAAGGT
CoxI_F	TGCTAGCCGCAGGCATTACT
CoxI_R	CGGGATCAAAGAAAGTTGTGTTT
Dars2_F	GGAATTAGCCAGGTCGTTGGA
Dars2_R	ACGAACCTTTTCCGGCTCAG
Fasn_F	CCCTTGATGAAGAGGGATCA
Fasn_R	ACTCCACAGGTGGGAACAAG
Fgf21_F	AGATCAGGGAGGATGGAACA
Fgf21_R	TCAAAGTGAGGCGATCCATA
Gdf15_F	CAACCAGAGCCGAGAGGAC
Gdf15_R	TGCACGCGGTAGGCTTC
Gpx1_F	CCACCGTGTATGCCTTCTCC
Gpx1_R	AGAGAGACGCGACATTCTCAAT
Hprt_F	GCCCCATGGTTAAGGTT
Hprt_R	TTGCGCTCATAGGCTTT
Mthfd2_F	CATGGGGCATATGGGAGATAAT
Mthfd2_R	CCGGGCCGTTCGTGAGC
Nfe2I2_F	TCCATTCCCGAATTACAGTGTCT

Table 3.6 Primer List. (cont.)

Primer Name	Sequence (5'-3')
Nfe2I2_R	GCCCACTTCTTTTTCCAGCG
Pdk4_F	CCCGCTGTCCATGAAGCAGC
Pdk4_R	CCAATGTGGCTTGGGTTTCC
Pparα_F	CTGAGACCCTCGGGGAAC
Pparα_R	AAACGTCAGTTCACAGGGAAG
Pparγ_F	TGCAGCTCAAGCTGAATCAC
Pparγ_R	ACGTGCTCTGTGACGATCTG
Sod1_F	CAAGCGGTGAACCAGTTGTG
Sod1_R	TGAGGTCCTGCACTGGTAC
Sod2_F	GCCTGCACTGAAGTTCAATG
Sod2_R	ATCTGTAAGCGACCTTGCTC

4. METHODS

4.1. Mouse Experiments

4.1.1. Animal Care

All animals were bred at Boğaziçi University Experimental Animal Breeding and Care Unit. Experimental procedures on mice were in compliance with the guidelines stipulated by the Republic of Turkey Ministry of Agriculture and Forestry and granted by "Boğaziçi Üniversitesi Kurumsal Hayvan Deneyleri Etik Kurulu BÜHADYEK)." Animals were raised in well-ventilated cages under 12 hours of light/dark cycle and maintained at 20°C - 24°C. The animals were weighed weekly, and standard food and water were given ad-libitum. The ketogenic diet intervention was started after weaning, and the study group had free access to food; the ingredients are shown in table 4.1. AICAR injection study group was administered with AICAR or vehicle (saline) starting from weaning with daily subcutaneous injection of 0.5 mg/day/gm of body weight into the lateral distal portion of the back. The cervical dislocation method was used to scarify animals.

Table 4.1. Very low carbohydrate ketogenic rodent diet

Ingredients	**gm**	***kcal* (%)**
Protein	17.6	10.4
Carbohydrate	0.2	0.1
Fat	67.2	89.5
Total		100
kcal/gm	6.76	

4.1.2. Survival Curve

Each mouse in the study groups was monitored weekly for their health conditions. Their death age was recorded, and mice with worsened conditions outreaching ethical limits were euthanized according to the responsible veterinarian's suggestion.

4.1.3. Phenotypic Experiments

4.1.4. Activity Cage

The experimental mouse was placed in the activity cage, and voluntary locomotor activity was recorded for 30 mins. The cage has two sets of infrared beam systems, counting the movements on the horizontal and vertical axis. All activities breaking infrared rays were recorded by the instrument.

4.1.5. Grip Strength

The muscle strength of animals was assessed by the grasping of the mice on the grid with their forelimbs and hindlimbs. Mice were held by their tail and pulled gently at a constant speed. The maximal grip force data in a pull was measured and recorded by the sensor. The procedure was repeated for each mouse five times at 1-minute intervals. The maximum and the minimum values were excluded, and their muscle strength was obtained from the average of 3 trials in the gram-force units.

4.1.6. Treadmill

The inclination angle of the treadmill was scaled on a 10° slope, and the electrical stimuli frequency and intensity were set to 200 msec/pulse, 3 Hz, and 1.22 mA to be kept consistent through training and testing. Mice placed in a separate lane on the treadmill were adapted to the treadmill exercise for two days at a constant speed (6.5 m/min) for 10 mins; after adaptation, the movement was repeated weekly. During the exercise, the initial speed of the platform was set to 6.5 m/min and gradually accelerated by 0.5 m/min every 3 mins.

The experiment was terminated when mice were considered exhausted, defined as ten falls into the electrical grid in a minute, and the covered distance was recorded.

4.1.7. RotaRod

Mice were adapted to the RotaRod system for two days before the experiment by being placed onto the horizontal rod lanes separately, and after 5 mins on the rod, the rod started to rotate with a constant speed of 5 rpm. Throughout the exercise, the rod was continuously accelerated for 5 min from a minimum of 2 rpm to a maximum of 50 rpm. The duration of their stay on the rod was observed, and the experiment was performed thrice at 20 mins time intervals.

4.1.8. Blood Glucose Measurement

A drop of blood was obtained from the lateral vein of the mice and applied directly to a glucose strip attached to the Accu-Check Glucometer. The glucose levels were monitored and recorded weekly for all study groups starting from the 3rd week of their age to the terminal stage.

4.1.9. Mouse Tissue Harvesting

For this study, the quadriceps and the gastrocnemius muscle tissues were harvested after the scarification of mice with cervical dislocation. Tissues were frozen immediately in liquid nitrogen for storage. For histology studies, one of the gastrocnemius muscles of each mouse was frozen in isopentane for 25 seconds and transferred to the tube in liquid nitrogen, later on, continued with OCT embedding. For mitochondria isolation, quadriceps muscle tissues were transferred to the ice-cold PBS-EDTA immediately after harvesting.

4.2. Genotyping

4.2.1. DNA Isolation from ear/tail biopsy

DNA was extracted from mouse ear or tail biopsies. Biopsies were incubated at 55°C in a thermoshaker overnight with 500 µl DNA Extraction Buffer and 5 µl Proteinase K. The following day 500 µl isopropanol was added to the tubes, and samples were centrifuged at 1500 rpm for 20 mins at 4°C. The supernatants were discarded, and 500 µl ice-cold 70% EtOH was added to the tubes, followed by centrifugation at 1500 rpm for 15 mins at 4°C, and the supernatants were discarded. After the samples were entirely dried from the remnant EtOH, pellets were resuspended with 50 µl ddH_2O in the thermoshaker for an hour at 37°C. Isolated DNAs were stored at 4°C for genotyping.

4.2.2. Polymerase Chain Reaction

PCR reactions were set up using *Cre* and *Dars2* primers to identify wild-type and knockout mice. The reaction mixes for each primer were prepared separately according to the parameters listed in the table 4.2, and conditions were applied as shown in the table 4.3.

Table 4.2. PCR Reaction Mix

1X Reaction Components	***Cre* & *Dars2***
DNA	1µl
ddH_2O	11.1 µl
GoTaq 5X Reaction Buffer	4 µl
dNTP Mix (1.25 mM)	1 µl
Forward Primer (10 µM)	0.8 µl
Reverse Primer (10 µM)	0.8 µl
$MgCl_2$	1.2 µl
Flexi-GoTaq Enzyme (5U/10 µl)	0.1 µl
Total Volume	20 µl

Table 4.3. PCR Conditions

	Temperature		Time		Cycle	
Steps	**Cre**	**Dars2**	**Cre**	**Dars2**	**Cre**	**Dars2**
Initial Denaturation	95°C	95°C	5 mins	5 mins	1	1
Denaturation	95°C	95°C	30 secs	30 secs	35	30
Annealing	62°C	60°C	30 secs	30 secs		
Extension	72°C	72°C	30 secs	45 secs		
Final Extension	72°C	72°C	5 mins	7 mins	1	1

4.2.3. Agarose Gel Electrophoresis

1% (w/v) agarose was dissolved in 1X TBE Buffer by heating in a microwave and transferred to a tray to solidify. After the gel was solidified, 3 µl 1kb DNA Ladder and 10 µl samples, including positive and negative controls, were loaded into the wells. The gel was run at 120V for 25 mins. When the run was completed, the gel was incubated in the Ethidium Bromide solution for 25 mins and imaged with GelDoc XR System.

4.3. mRNA Levels Quantification

4.3.1. RNA Isolation from Mouse Skeletal Muscle

RNA was extracted according to the Zymo Research Direct-zol RNA MiniPrepPlus Kit protocol. 600 µl TRIzol Reagent was added into Roche tubes with magnetic beads. 50 mg of quadriceps muscle tissues were cut into small parts with a scalpel and transferred to the tubes. Tissues were homogenized twice by the MagNa LYser at 6500 rpm for 30 secs. Samples were centrifuged for 5 mins at 1500 rpm at 4°C (all centrifuge steps for this experiment were held at 1500 rpm at 4°C), and supernatants were transferred into Eppendorf tubes. 600 µl 100% EtOH was added to the supernatant. The mixture was transferred to the

Zymo-Spin IIICG column and centrifuged for 30 secs, and the flow through was discarded. 400 µl RNA Wash Buffer was added to the column and centrifuged for 30 secs. 275 µl Nuclease-free water was mixed with DNaseI powder, 5 µl of which was added to 75 µl DNA Digestion Buffer for each sample and added to the column. The samples were incubated at RT for 15 mins; later, 400 µl RNA Prewash Buffer was added to the column and centrifuged for 30 secs (x2). 700 µl RNA Wash Buffer was added to the column and centrifuged for 2 mins, and the flow through was discarded. 50 µl Nuclease-free water added column was centrifuged for 2 mins. Nanodrop was used to measure sample concentration, purity, and integrity. Samples were stored at -80^{0}C.

4.3.2. cDNA Synthesis

cDNAs were synthesized using the iScript^{TM} cDNA Synthesis Kit, according to the manufacturer's protocol. The reaction conditions are given in Tables 4.4 and 4.5.

Table 4.4. cDNA Synthesis Mix

Components	Quantity
5X iScript Reaction Mix	4 µl
iScript Reverse Transcriptase	1 µl
Nuclease-free Water	Variable (15-X µl)
RNA Template	Variable (X µl)
Total Volume	20 µl

Table 4.5. cDNA Synthesis Reaction Conditions

Steps	Temperature	Time	Cycle
Priming	25°C	5 min	1
Reverse Transcription	46°C	20 min	1
Reverse Transcriptase Inactivation	95°C	1 min	1

4.3.3. Quantitative PCR reaction

Primers were mixed with nuclease-free water according to the manufacturer's recommendations. The qPCR reaction mix was prepared, and the reaction was performed as shown in Tables 4.6 and 4.7, respectively. For each gene, one negative control was loaded to the 96 well-plate. The relative gene expression levels were normalized against *Hprt*.

Table 4.6. qPCR Component

Components	Quantity
DNA	2 µl
Nuclease-free Water	2.5 µl
Forward Primer	0.25 µl
Reverse Primer	0.25 µl
RealQ Plus 2X Master Mix	5 µl
Total Volume	10 µl

Table 4.7. qPCR Conditions

Steps	Temperature	Time	Cycle
Initial Denaturation	95°C	15 mins	1
Denaturation	95°C	15 secs	4^0
Annealing	60°C	15mins	
Extension	72°C	15 secs	

4.4. Protein Level Quantification

4.4.1. Protein Isolation from Mouse Skeletal Muscle

500 µl Organ Lysis Buffer and quadriceps muscle tissues, approximately 50 mg, were added to the Roche tubes with magnetic beads. Tissues were homogenized in the lysis buffer twice with MagNa LYser at 6500 rpm for 30 secs. Samples were centrifuged at 1500 rpm

for 45 mins at 4°C, and supernatants were transferred into Eppendorf tubes and stored at -80°C.

4.4.2. Protein Concentration Quantification

1:10 and 1:20 dilutions were prepared following the manufacturer's protocol (BioRad DC Protein Assay) with 2 µl isolated protein lysates and 18 µl and 38 µl ddH_2O, respectively. 5 µl of samples and BSA standards were loaded as duplicates into 96 well-plate. A' solution was prepared freshly with the ratio of 1 µl S solution and 50 µl A solution, 25 µl of A' and 200 µl B solutions were added to the wells. The plate was incubated at RT for 15 mins, and a plate reader was used to measure OD values at 750 nm.

4.4.3. Western Blot

Western Blot Analysis was performed by the lysates obtained from mice quadriceps. The reaction mix was prepared with 50 µg protein lysate, 4X NuPage Reaction Buffer, and 10X Reducing Agent, and a variable amount of ddH_2O was added to reach a final volume of 11 µl. Samples were incubated at 70°C for 10 mins. Polyacrylamide gel was prepared in two layers, resolving and stacking, and wells were loaded with a 3 µl protein ladder and 10 µl samples. The protein extracts were separated electrophoretically on 10% gel and wet transferred to a nitrocellulose membrane. For the transfer, Whatmann filter papers, sponges, nitrocellulose membrane, and the gels were soaked in 1X transfer buffer, and the transfer sandwich was prepared in order of sponge, Whatmann filter paper, NC membrane, the gel, Whatmann filter paper, and sponge, in every layer, the bubbles were eliminated with a roller. Ponceau S. staining method was used to examine the quality of the transfer, which was later rinsed with PBS-T. For blocking, the membrane was shaken in 5% milk powder and PBS-T solution on an orbital shaker, followed by washing the membrane with PBS-T 3 times for 5 mins (all washing steps were held the same). The membrane was incubated in primary antibody overnight at 4°C and then washed again. The secondary antibody incubation was carried out for an hour at RT, followed by membrane wash. For visualization with SynGene G-Box Instrument, the membrane was saturated with 1:1 ECL or Sirius:Peroxide solution and the images were analyzed with ImageJ Software.

4.5. Mitochondria Isolation from Mouse Skeletal Muscle

Harvested quadriceps muscle tissues were immediately transferred to the ice-cold PBS-EDTA. Using scissors, tissues were cut into small pieces and moved into a falcon containing 1 ml Trypsin, where they were incubated for 30 mins on ice. The sample was centrifuged at 200 g for 5 mins at 4°C, the supernatant was discarded, and the pellet was homogenized with a glass homogenizer by hand in 5 ml IMB1 Buffer and transferred into a new falcon. 5 ml IMB1 Buffer was added to the mixture and centrifuged at 700 g for 10 mins at 4°C. The supernatant was transferred to a new falcon and centrifuged for 10 mins at 8000 g at 4°C. The supernatant was discarded, and the pellet was resuspended with 5 ml IBM2. The sample was centrifuged for 10 mins at 8000 g at 4°C. The supernatant was discarded, and the pellet was resuspended with 10 µl IBM2. The mitochondria concentration was measured as explained in protein concentration quantification.

4.5.1. Oxygen Consumption Rate and H_2O_2 Production Measurement

0,13 mg mitochondria isolated from WT and KO mice quadriceps were used to measure oxygen consumption and H_2O_2 production rates via the Oroboros-O2k instrument. For the measurement of oxygen consumption and H_2O_2 production with Amplex®UltraRed, the fluorescence sensors with green filters were inserted into the O2k chambers. According to the instrument protocols, air and H2O2 calibrations were conducted by adding the Mitochondria Respiration Buffer to the chambers. After calibrations, isolated mitochondria are added, the amount of which was determined as described in 4.4.2. SUIT-006-D048 protocol was followed for H_2O_2 production during forward electron transport. 5 mM Pyruvate, 2 mM Malate, 2.5 mM ADP, 5 nM Oligomycin, 0.5 µM CCCP (repeated for some samples) and 2.5 µM Antimycin A, along with 0.1 µM H_2O_2 titration (thrice) were added to chambers. For Hydrogen Peroxide measurement during reverse electron transport, SUIT026-D064 protocol was followed, including the addition of 10 mM Succinate, 0.5 µM Rotenone, 2.5 mM ADP, 2.5 µM Antimycin A with thrice 0.1 µM H_2O_2 titration. Data analysis was conducted according to the excel templates offered by the manufacturer.

4.5.2. Membrane Potential Measurement with Safranin

Mitochondrial membrane potential was measured with safranin by the Oroboros-O2k instrument. Fluorescence sensors with blue filters were attached to the chambers to detect changes in safranin level. After safranin calibration by adding 1µl safranin (4 times) into chambers, 0,13 mg isolated mitochondria were added. SUIT-021-D036 protocol was conducted with the addition of 10 mM Glutamate, 2 mM Malate, 2.5 mM ADP, 10 mM Succinate, 0.5 µM Rotenone, 5 nM Oligomycin, 0.5 µM CCCP (repeated for some samples) and 2.5 µM Antimycin A. excel template offered by the manufacturer was used for data analysis.

4.6. Histology of Mouse Skeletal Muscle

4.6.1. Sectioning of Mouse Skeletal muscle

The Cryomold chamber was filled with OCT, and frozen gastrocnemius muscle tissue was embedded. The Cryomold chamber was placed on the metal rack precooled with liquid nitrogen. Frozen sections were cut in 8 µm thickness with a cryostat and placed on a positively charged slide. The slide was air-dried for 30 mins before the staining.

4.6.2. H&E Staining

The slide was incubated in Hematoxylin for 5 mins, then Hematoxylin was briefly washed with 0.1M HCl, and the slide was rinsed under running water for 2 mins. The slide was incubated in Eosin Y for 20 secs and rinsed under running water quickly. For dehydration, the slide dipped into 70% and 90% EtOH 15 times and 99% EtOH 20 times. The slide was incubated in Xylene for a minute, air-dried, and mounted with DPX and a coverslip.

4.6.2. COX-SDH Staining

The edge of the slide was drawn with a PapPen. For each slide, 800 µl DAB and 200 µl Cytochrome C were mixed and added to the slide. The slide was incubated for 2 hours at 37°C. After the incubation, the slide was shaken thrice for 30 secs in PBS. The mixture of 800 µl NBT, 100 µl Sodium Succinate, 100 µl PMS and 10 µl Sodium Azide was added to the slide and incubated for 20 mins at 37°C. The slide was washed with PBS thrice and dehydrated through incubation of 4 mins in 95% of EtOH and 10 mins of 99% EtOH. The slide was air-dried and mounted with DPX and a coverslip.

5. RESULTS

5.1. The Generation of Mitochondrial Translational Deficient Mouse Model

The floxed *Dars2* mouse (*Dars2*$^{LoxP/LoxP}$), carrying LoxP sites at the second intron and the third exon, was crossed with the transgenic mouse, expressing Cre recombinase under Human alpha-actin 1 (*ACTA1*) promoter (*Dars2*$^{LoxP/LoxP,\ +/+}$ x *Dars2*$^{+/LoxP,\ +/Cre}$). Both models were obtained from Prof. Aleksandra Trifunovic's group in Cologne Excellence Cluster in Aging and Aging-Associated Diseases (CECAD), Cologne, Germany (Dogan et al., 2014). The resulting offspring showed Mendelian proportions with a 1/4th ratio of homozygous mutant mice. Due to no detection of worsening, the heterozygous mice were not studied in this project. Genotypes of the study groups were examined by PCR and agarose gel electrophoresis. DARS2 depletion was confirmed by the attenuation of *Dars2* transcript levels in the skeletal muscle of mKO but not in WT mice.

5.2. Phenotypic Characterization of the Mouse Model

Previous research from our lab revealed that mKO mice had severe mitochondrial dysfunction in skeletal muscle, shortening their lifespan to 54 days Figure 5.1. The loss of fur, flushing, and halting of growth and body weight were detected in mKOs. The difference in body weight was observed after weaning and became more evident over time as the weight gain stopped at 4-5th weeks of age and weight loss started Figure 5.1. The data is not distinguished between sexes due to the similarities in results of phenotypic and molecular experiments (Yılmaz, 2022).

The behavioral experiments were repeated to increase the mouse numbers and confirm the previously observed phenotypic results. DARS2-deficient mice showed evidence of skeletal muscle atrophy due to the smaller size of the quadriceps and the gastrocnemius muscle tissues, consistent with the increase in the transcript levels of *Atrogin* and *Murf1*, atrophy markers, as a sign of myopathy and lower muscle-to-body weight ratio compared to WT mice (Yılmaz, 2022).

The mouse model was subjected to various behavioral tests for phenotypical characterization, including voluntary movement, muscle strength, motor performances, and locomotor activities. The phenotypic experiments were performed weekly, starting from 3 weeks of their age.

The voluntary activities of the experimental groups in horizontal and vertical directions were counted via the Ugo Basile® activity cage for 30 mins. The data on vertical movement is excluded because of the short height of mKOs; infrared lasers failed to capture their standing motions. mKOs displayed a significantly lower number of spontaneous movements in the horizontal direction than WT littermates throughout their lives, indicating their incapability of moving actively due to skeletal muscle atrophy Figure 5.1.

Grip strength assay was conducted with an Ugo Basile® grip strength meter. In their third week, mKOs applied insignificantly less strength ($p=0.06$) than the control group. However, the difference between the experimental groups increased in the following weeks, supporting the observation that mKOs have decreased muscle strength Figure 5.1.

To test the endurance and exercise intolerance of mKO mice, animals were forced to run on the treadmill. The running performance of mKOs was significantly less than the controls and progressively regressed as they aged. Throughout the study, the running distance of WTs was around 1000 m, while the running distance of mKOs was 135 m in the third week of their age and successively diminished to 4m at the 7^{th} week of age, supporting the results on lower exercise performance compared to WTs Figure 5.1.

The motor coordination of animals was observed with the RotaRod as the final behavioral test. Although mKOs showed less voluntary movement, muscle strength, and exercise intolerance than their WT littermates, motor coordination and balancing abilities did not indicate a significant difference between the experimental groups. The results conform with the results from the previously studied project, corroborating that DARS2 depletion leads to severe and progressive mitochondrial myopathy phenotype Figure 5.1.

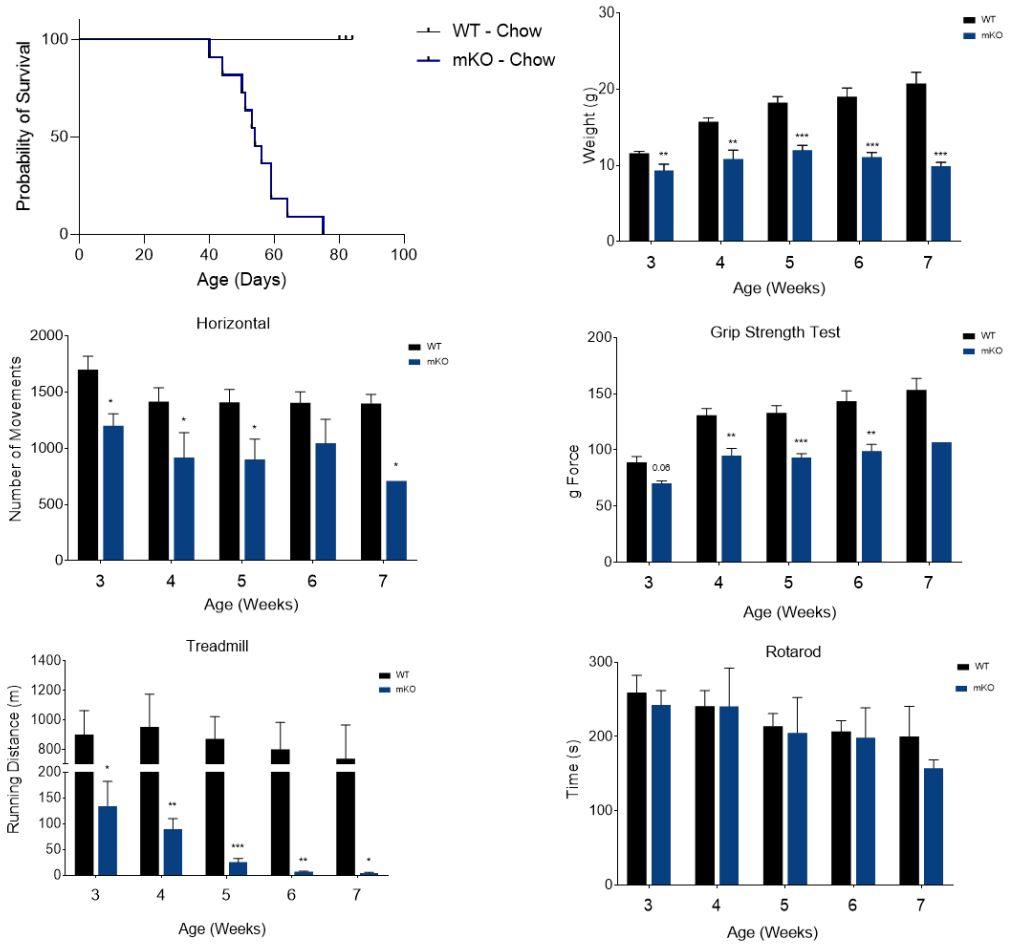

Figure 5.1. Survival curve of skeletal muscle-specific DARS2 KO mouse model (n=6-11) and results of Phenotypic Assays; Weight, Activity Cage (horizontal), Treadmill, Rotarod (n=3-14). Error bars represent mean ± SEM. (Student's t-test: *p<0.05, **p<0.01, ***p<0.001).

As the atrophy marker levels were increased, and the body and skeletal muscle sizes were much smaller in mKOs, we wanted to weigh the gastrocnemius muscle to understand the reason behind the reduction of muscle size. The gastrocnemius muscle weights obtained from both WT and mKO animals at 6 weeks of age were normalized to their body weight. An insignificant reduction has been observed in mKOs Figure 5.2.

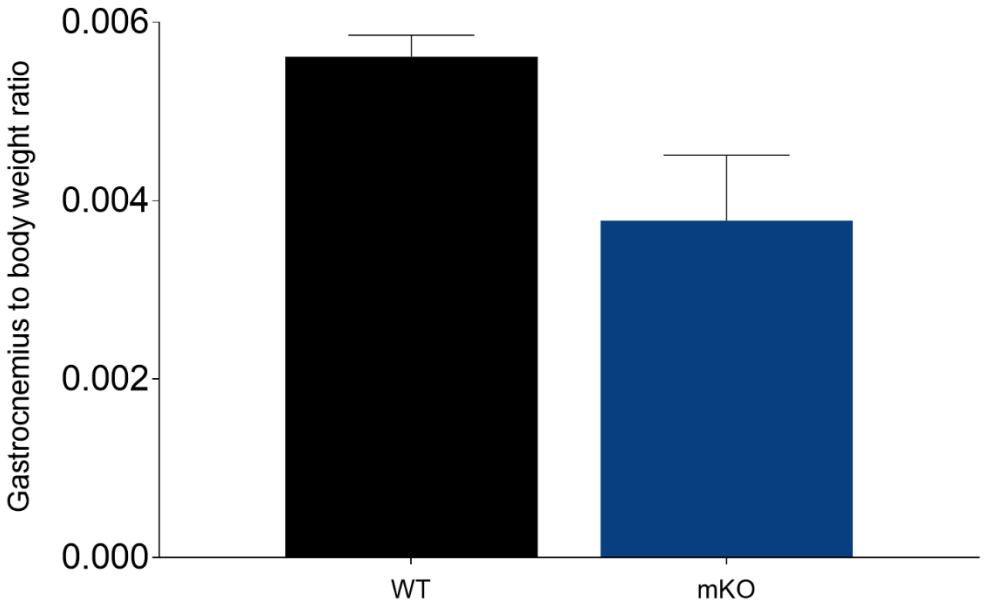

Figure 5.2. The gastrocnemius: body weight ratio of 6 weeks old mKO and WT mice (n=3). Error bars represent mean ± SEM. (Student's t-test: *p<0.05, **p<0.01, ***p<0.001).

5.3. Histology of mKO-Skeletal Muscle

Skeletal muscle is a highly adaptive tissue that can alter its mass and fiber type in response to exercise, diet, aging, and disorders; characterization of the changes in composition and size has been used in the diagnosis of diseases. The loss of muscle mass is associated with atrophy and proportional loss of muscle strength, which can be caused by the decrease in the number and/or size of the myofibers. Whereas 'healthy' myofibers have peripheral nuclei and intact sarcoplasm and sarcolemma, the presence of centralized nuclei is a sign of muscle regeneration (Dogan et al., 2018). The morphological analysis of transverse skeletal muscle sections of WT and mKO mice with H&E staining revealed that DARS2-depleted mKO myofibers had peripheral nuclei; interestingly, muscle regeneration was not activated as a stress response in the mouse model. While control mice displayed homogeneously distributed fiber size, we observed a significant decrease in the cross-sectional area of DARS2-depleted mice myofibers, indicating skeletal muscle size was not

only affected by the smaller size of the animal but also by the decrease in the size of myofibers, which is an indicator of mitochondrial myopathy Figure 5.3a. In atrophy cases, besides the reduction of the muscle fiber size, their ability to function properly is lost, supporting our observation of the loss of muscle strength in mKO.

The RC activity can be assessed by cytochrome c oxidase (COX)/succinate dehydrogenase (SDH) staining. COX-positive fibers are observed in dark brown, and SDH-positive fibers are in intense blue color. In case of reduced complex activity, the stains are less precipitated in the cells, resulting in lighter fiber colors. However, due to mitochondrial dysfunction, in COX-negative fibers, the detection of SDH precipitation is higher since entire CII subunits are encoded in nuclear DNA. The presence of COX-deficient/SDH-positive cells is indicative of mitochondrial muscle manifestation (Pfeffer & Chinnery, 2013). The histochemical activity analysis for COX revealed that mKO muscle fibers had lighter brown precipitation, indicating a detectable decrease in COX activity. However, SDH staining showed that mKO fibers were strongly stained with blue precipitant, a representative of high SDH levels. We observed the segmentation of blue precipitant in myofibers as a result of COX/SDH double staining, which can be explained by the presence of COX-intermediate fibers, representing the transition from normal RC to deficient fibers. COX/SDH histochemical analysis revealed COX deficiency in mKO with the prevalence of SDH-positive fibers as a result of mitochondrial RC dysfunction Figure 5.3b.

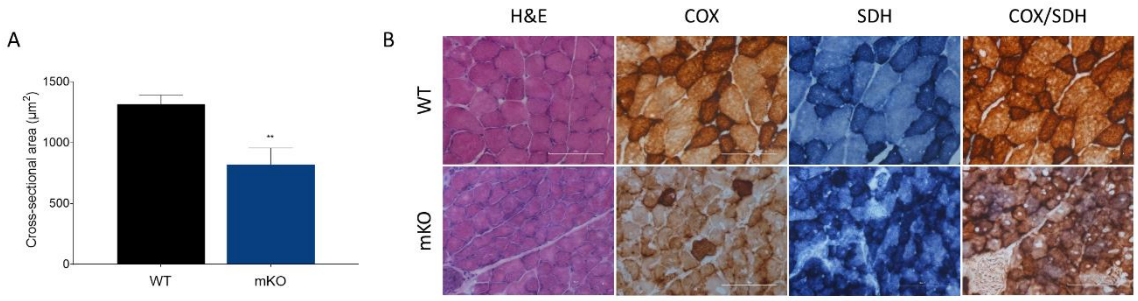

Figure 5.3. Histological and histochemical analysis of WT and muscle fibers (n=3-6). (a) Analysis of the cross-sectional area of skeletal muscle fibers. (b) Histochemical analyses of Hematoxylin and Eosin, COX, SDH, and COX/SDH stainings of skeletal muscle sections of 6–7-week-old WT and mKO animals. Error bars represent mean ± SEM. (Student's t-test: *p<0.05, **p<0.01, ***p<0.001).

5.4. Molecular Characterization of the Mouse Model

Hypoglycemia is a common feature observed in patients with mitochondrial disorders; therefore, detecting lower blood glucose levels on mKOs was expected (Ashfaq et al., 2021). Further examination of blood sugar levels showed that hypoglycemia progressively developed as the mKOs got older, and at the final stages, it dropped approximately 70 mg/dL (Yılmaz, 2022).

As the skeletal muscle fiber size and RC activity are highly dependent on the balance between protein synthesis and degradation, we examined the changes in protein and mRNA levels in both WT and mKO animals. The analysis of OXPHOS protein subunits indicated a possible mitochondrial biogenesis induction in the skeletal muscle of mKOs as the subunits of CI (NDUFA9), CIII (UQCRC2), and CIV (COX IV) were reduced, whose functions are also highly dependent on mtDNA encoded subunits, whereas the CII (SDHA) and CV (ATP5A) subunit levels were elevated; the entire CII and F_1 subunit of CV are encoded in the nuclear genome. Further examination of the levels of proteins in mitochondrial biogenesis directly, PGC1α, and phosphorylated AMPK (p-AMPK), or indirectly, strengthen the indication. Except for PGC1α, the level of p-AMPK along with TFAM, HSP60, VDAC1, and TOM20, which are associated with the number of mitochondria, were increased in mKOs compared with their WT littermates. PGC1α levels were not altered in a previous study (Yılmaz, 2022); however, in this study insignificant decrease in its level was observed in terminal-stage KO mice.

As mitochondrial homeostasis is balanced by mitochondrial biogenesis and its turnover, the protein level of autophagy markers was observed. An increase in the P62 level indicates an accumulation of ubiquitinated proteins, yet impairment of the degradation of these proteins by autophagosomes due to the decline in the LC3BI/LC3BII ratio. Moreover, the protein levels of antioxidant response markers NFE2L2 and SOD2 were increased, whereas the transcript levels, including, *Gpx1*, were reduced. The inconsistency in transcript and protein levels of antioxidant response-related genes suggests the involvement of ROS or impairment of protein degradation and autophagy. In *C. elegans*, the proteotoxicity induces unfolded protein response, whose counterpart in mammalians is ISR^{mt}. The induction of ISR^{mt} has been observed in our myopathy model via an increase in the level of

phosphorylated eIF2α and PYCR1 proteins and *Chop, Aldh18a1, Mthfd2, Gdf15,* and *Fgf21* transcripts (Yılmaz, 2022). On the other hand, in addition to our previous results, *Nrf2* protein and transcription levels were lower in mKOs, which might affect the reduction of RC levels Figure 5.4.

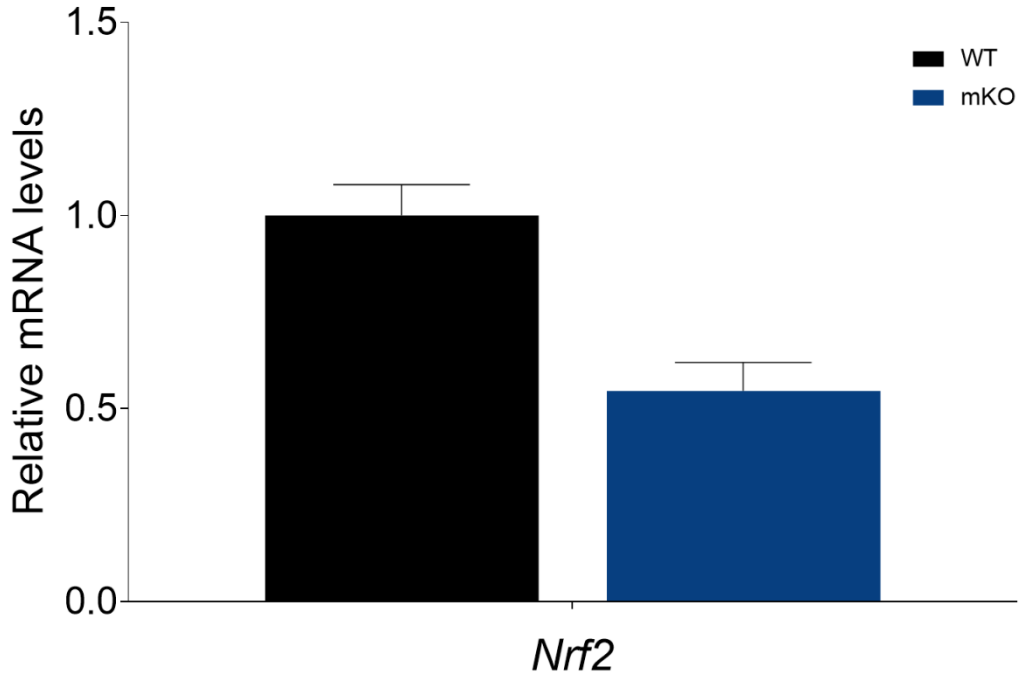

Figure 5.4. Transcript Levels of *Nrf2* in WT and mKO mice (n=4-5). Error bars represent mean ± SEM. (Student's t-test: *p<0.05, **p<0.01, ***p<0.001).

Next, we examined the effect of DARS2 depletion on oxygen consumption rates (OCR) in the skeletal muscle of mKO and WT mice. When supplemented with pyruvate and malate, CI substrates, mitochondria of DARS2-ablated skeletal muscles showed a significantly lower level of CI-linked respiration compared to the skeletal muscle of WT mice, which is also mirrored in ADP-stimulated, state 3 respiration. The difference in OCR in state 4 respiration rate under the presence of oligomycin, an inhibitor of CV, skeletal muscle mitochondria of mKO mice were detected to respire less than the controls, although it was not significant. With the uncoupler supplementation, mKO mitochondria exhibited reduced OCR, though the difference was insignificant Figure 5.5a.

To examine the CII-linked respiration in skeletal muscle mitochondria of mKO and WT mice, we measured the OCR, first in the presence of succinate, CII substrate, later rotenone, an inhibitor of CI, and lastly ADP. Mitochondria of mKO skeletal muscle showed significantly reduced OCR after each supplementation Figure 5.5b. Overall, OCR's data analysis indicated that DARS2-depleted skeletal muscle mitochondria had decreased CI and CII-linked respiration than WT mitochondria.

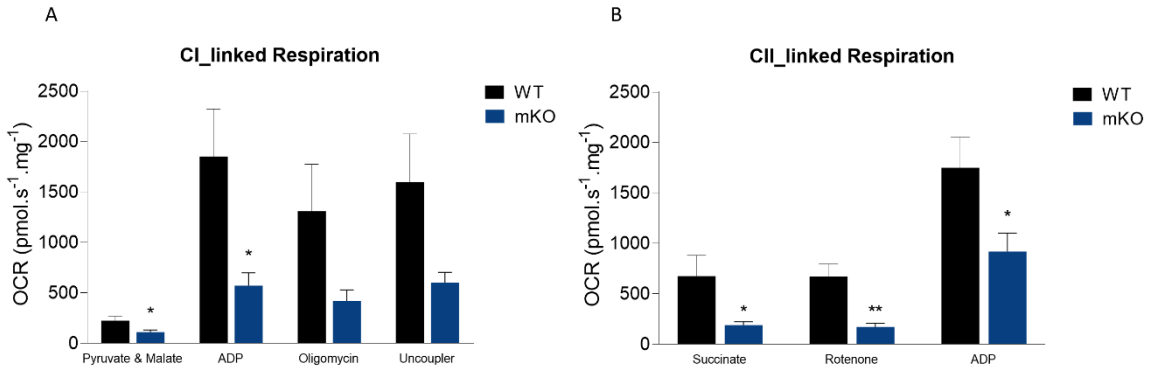

Figure 5.5. The Oxygen Consumption Rate (OCR) of (a) CI-linked respiration and (b) CII-linked respiration in the skeletal muscle of WT and mKO mice (n=8-9). Error bars represent mean ± SEM. Asterisks denote the statistical significance of p values, comparing each group to their relative controls as indicated in the graph. (Student's t-test: *p<0.05, **p<0.01, ***p<0.001).

H_2O_2 production rates of skeletal muscle mitochondria of mKO and WT mice were measured during CI and CII-linked respiration. We detected increased H_2O_2 production under CI substrate supplementation in DARS2-ablated mitochondria. No significant difference was observed in ADP, oligomycin, or uncoupler presence. However, antimycin A addition to the live mitochondria, which disrupts cellular respiration by binding CIII, resulted in decreased H_2O_2 production in mKO skeletal muscle Figure 5.5a.

In the presence of succinate, reverse movement of electrons due to over-reduced ubiquinone causes ROS production, which was significantly less in mKO mitochondria than in controls. Rotenone supplementation showed an apparent reduction in H_2O_2 flux in mKO and WT mitochondria. When antimycin A added, H_2O_2 production was significantly decreased in DARS2-depleted skeletal muscle mitochondria Figure 5.6b.

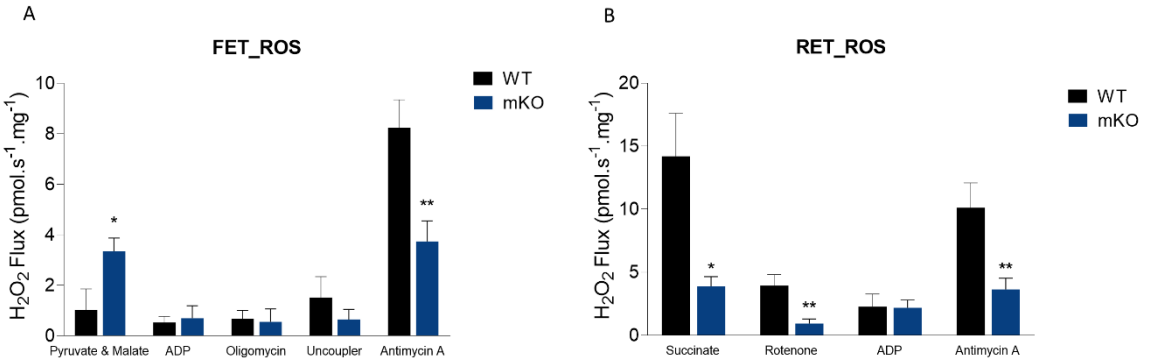

Figure 5.6. The ROS production level during (a) the Forward Electron Transfer (FET) process and (b) the Reverse Electron Transfer (RET) process in the skeletal muscle of WT and mKO mice (n=8-9). Error bars represent mean ± SEM. Asterisks denote the statistical significance of p values, comparing each group to their relative controls as indicated in the graph. (Student's t-test: *p<0.05, **p<0.01, ***p<0.001).

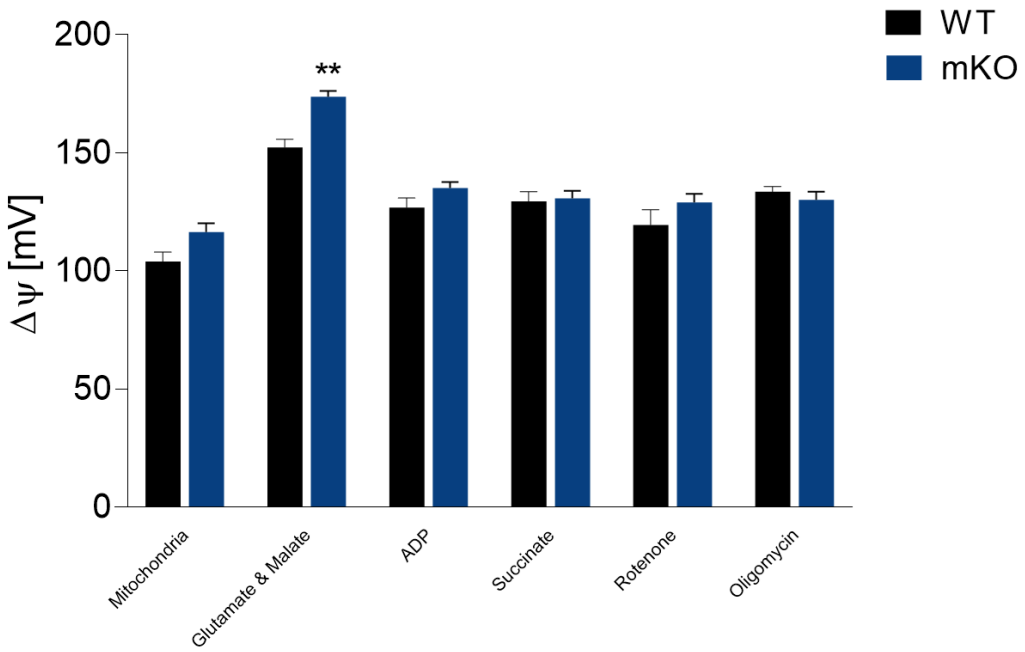

Figure 5.7. The analysis of mitochondrial membrane potential in the skeletal muscle of WT and mKO mice (n=4). Error bars represent mean ± SEM. Asterisks denote the statistical significance of p values, comparing each group to their relative controls as indicated in the graph. (Student's t-test: *p<0.05, **p<0.01, ***p<0.001).

Finally, the mitochondrial membrane potential differences in the skeletal muscle mitochondria of WT and mKO mice were evaluated. A substantial increase in the membrane potential during forward electron transfer was detected in the skeletal muscle of DARS2-depleted mice compared to their controls after glutamate and malate addition, CI substrates. No difference was detected in membrane potential after the ADP and CII stimulation, with succinate supplementation or after the inhibition of CI and CV by rotenone and oligomycin, respectively Figure 5.7.

5.5. Mitochondrial Myopathy Treatments

5.5.1. Ketogenic Diet Intervention

We administered KD or Chow Diet (CD) to the WT and mKO mice after weaning until the sacrification. The consequences of diet intervention were studied to understand the possible amelioration potential of KD on mitochondrial myopathy progression and the severity of the mouse model's phenotype.

5.5.2. Effects of KD on Phenotype

We first analyzed the lifespan of the KD-fed study groups; interestingly, KD intervention further shortened the lifespan of mKOs to 42 days. The study groups were regularly monitored for weight and exercise performance during the intervention. There was no difference in body weight or exercise capability between CD- and KD-fed mKOs. However, we observed a significant increase in the number of movements in the KD-fed WT group compared to their controls, starting from 5 weeks old. The rate of the difference stayed the same throughout the study Figure 5.8a.

Of note, we have not performed behavioral experiments in the lifespan cohort to eliminate possible adverse and/or beneficial effects. No difference in exercise capability was detected in mKOs due to diet intervention; the KD-fed mKO study group, which exercised regularly every week, lived longer than the life span test group, highlighting the beneficial effects of exercise for mitochondrial myopathy cases. Exercised-based therapy is still under

debate; the effects of exercise are highly dependent on the disease type and patient (Zeviani, 2008).

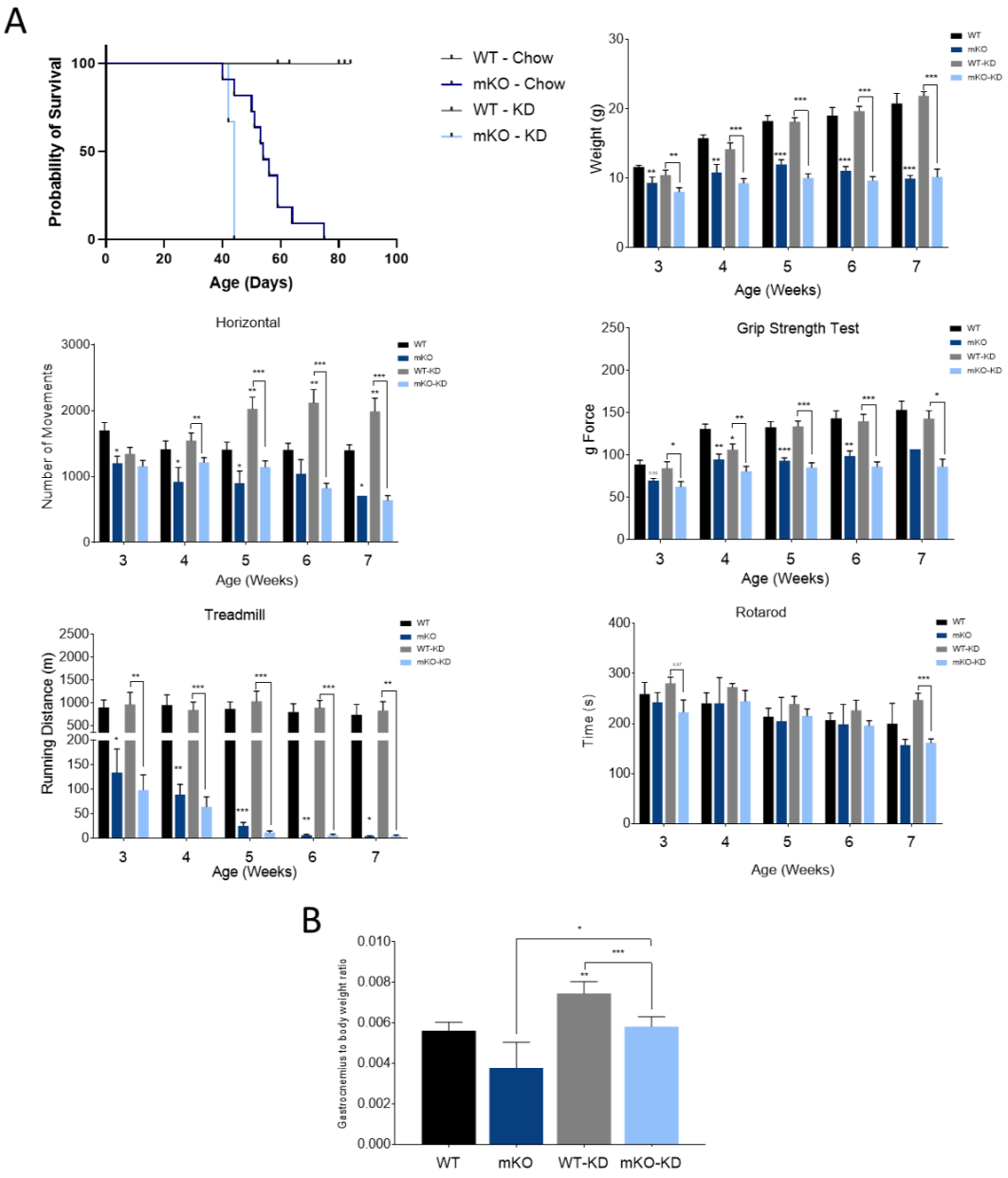

Figure 5.8. Survival curve of (a) KD-treated WT and skeletal muscle-specific DARS2 KO mouse model (n=2-11) and results of Phenotypic Assays; Weight, Activity Cage (horizontal), Treadmill, Rotarod (n=3-14). (b) The gastrocnemius to body weight ratio of chow and KD-treated animals. Error bars represent mean ± SEM. (Student's t-test: *p<0.05, **p<0.01, ***p<0.001).

Even though there was no difference in the body weights of KD-fed WT and mKO animals compared to their respective controls, the gastrocnemius-to-body weight ratio was significantly increased in both of the KD-fed groups, suggesting KD intervention elevated skeletal muscle mass Figure 5.8b.

5.5.3. Effects of KD on Skeletal Muscle Histology

Since the gastrocnemius-to-body weight ratio was increased in KD intervention groups, we examined the histology of myofibers from 6-7 weeks old mice fed with CD or KD to investigate the reason behind the change. The cross-sectional area of KD-fed groups did not show a difference in comparison to their controls, indicating the increase in the ratio was not a result of an increase in the myofiber size Figure 5.9a.

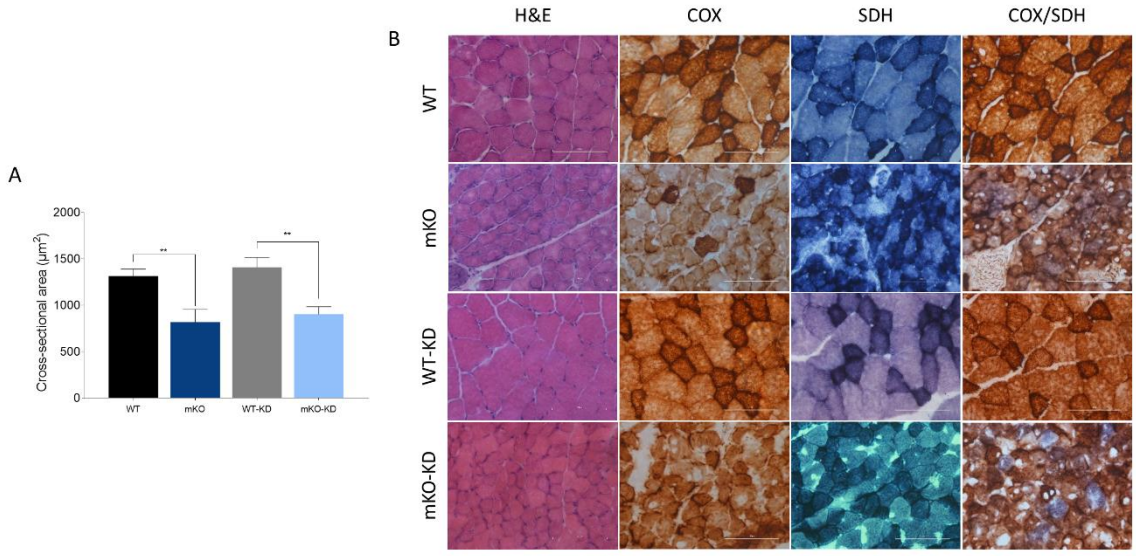

Figure 5.9. Histological and histochemical analysis of KD-treated WT and mKO muscle fibers (n=3-6). (a) Analysis of the cross-sectional area of skeletal muscle fibers. (b) Histochemical analyses of Hematoxylin and Eosin, COX, SDH, and COX/SDH stainings of skeletal muscle sections of 6–7-week-old WT and mKO animals. Error bars represent mean ± SEM. (Student's t-test: *p<0.05, **p<0.01, ***p<0.001).

Another way to enhance skeletal muscle mass is to elevate the number of myofibers. Therefore, we examined the nucleus locations for the induction of muscle regeneration.

Interestingly, we did not observe centralized nuclei on myofiber sections of KD intervention study groups; however, the sections were obtained from 6-7 weeks-old mice, which was the lifespan of mKOs. Muscle regeneration might have been induced in the early weeks of KD intervention; therefore, further investigation into skeletal muscle regeneration in younger KD-fed mice is needed Figure 5.9b.

The histochemical staining for COX activity revealed that KD intervention in the WT group showed increased reaction to COX, indicating recovery of COX levels and possible induction of mitochondrial biogenesis. However, there was no increase detected in SDH activity in the KD-fed WT group compared to their controls. We observed more homogenous precipitation in SDH-positive myofibers of KD-fed mKOs, which might indicate complete RC deficiency in myofibers, along with darker COX staining Figure 5.9b.

5.5.4. Effects of KD on Molecular Level

The blood glucose levels of CD or KD-fed mice were monitored weekly. Even though there was an insignificant increase in blood sugar levels of the KD-fed WT group in comparison to their controls, KD intervention in mKOs did not cause any change or amelioration in hypoglycemia progression Figure 5.10.

To obtain an understanding of the effects of KD on phenotype and skeletal muscle histology and the mouse model, we measured the protein levels of RC subunits. We observed upregulation of NDUFA9, a subunit of CI, in mKO mice. The increase in CI protein levels in mKOs might reflect mitochondrial biogenesis induction, and most CI subunits are nuclear encoded. The Western Blot analysis of RC subunits of KD-treated WT mice showed an insignificant increase in UQCRC2 (CIII), NDUFA9 (CI), and COX IV (CIV) subunits. In contrast, the entire nuclear encoded CII (SDHA) and F_1 domain of CV (ATP5A) subunits did not differ, indicating KD treatment upregulated expression of mitochondrial encoded subunits. In the skeletal muscle samples of KD-fed mKO mice, SDHA levels increased significantly, confirming our histochemical analysis results. KD treatment did not affect the amount of OXPHOS subunits of CI, CIII, CIV, and CV Figure 5.11.

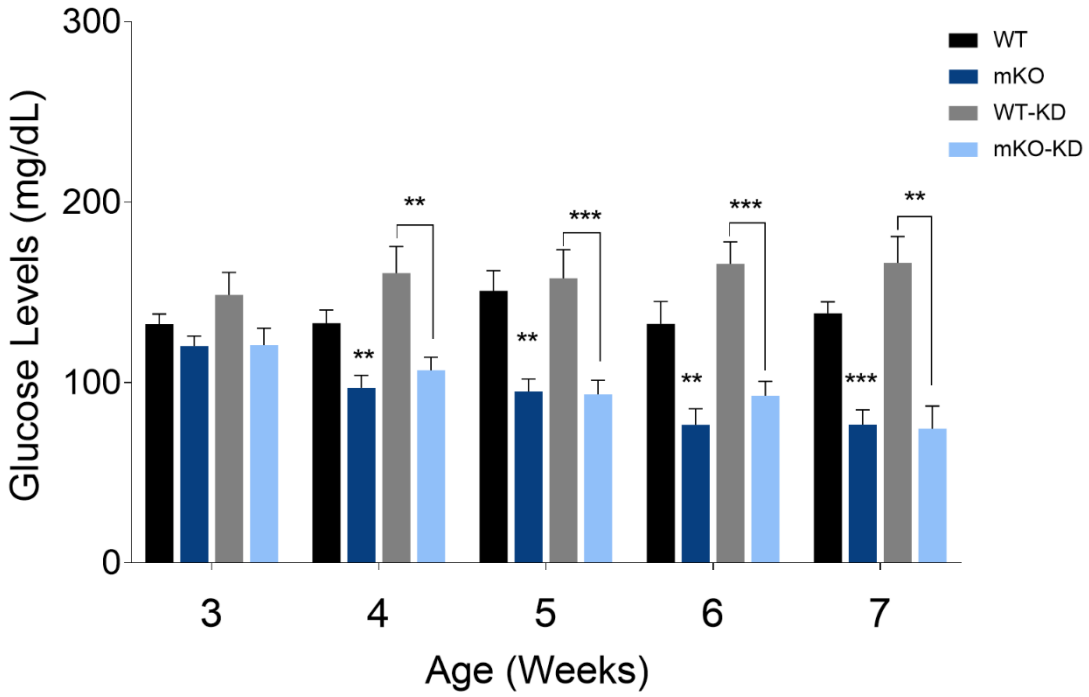

Figure 5.10. The glycemic levels of CD and KD-fed mice (n=7-13). Error bars represent mean ± SEM. (Student's t-test: *p<0.05, **p<0.01, ***p<0.001).

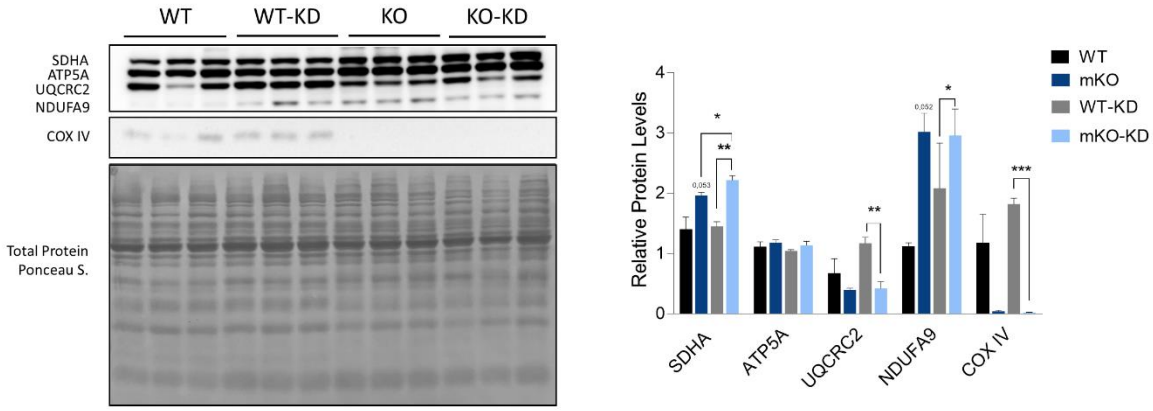

Figure 5.11. The Western Blot analysis (left) and the relative amount (right) of respiratory chain complexes I (NDUFA9-36kDa), II (SDHA-70kDa), III (UQCRC2-45kDa), IV (COX IV-15kDa) and V (ATP5A-55kDa) (n=3). Error bars represent mean ± SEM. Asterisks represent the statistical significance of p values. (Student's t-test: *p<0.05, **p<0.01, ***p<0.001).

We were interested in understanding the possible effect of KD treatment on mitochondrial biogenesis in WT and mKO mice. KD-fed WT animals showed a clear increase in TFAM and an almost significant (P=0.054) increase in HSP60 protein levels. TFAM, as a transcription factor for mtDNA, the amount is directly associated with the amount of mtDNA, thus its function in inducing mtDNA accessibility (Larsson et al., 1998). The mitochondrial chaperon HSP60 (mitochondrial Heat Shock Protein 60) is in charge of folding proteins imported to mitochondria (Voos & Röttgers, 2002). These results showed that KD treatment increased mtDNA copy number and the need for mitochondrial chaperons. However, the mitochondrial genome encoded CIV subunit *Cox1* transcript levels remained unchanged, and we did not detect a difference in the protein and transcript levels of *Pgc1α*, the master regulator of mitochondrial biogenesis. Even though AMPK levels were increased in KD-fed WT mice, activated AMPK and p-AMPK/AMPK ratios were unchanged in correlation with PGC1α levels. No difference was observed in NRF2 levels, supporting the unaltered level of PGC1α and nuclear-encoded RC subunits. Interestingly, the amount of VDAC was significantly reduced. VDAC is a mitochondrial membrane protein; a decrease in the level might represent a reduction in the number of mitochondria Figure 5.12a.

AMPK activation was stimulated in mKOs, and KD treatment resulted in further but insignificant increased phosphorylation of AMPK, consistent with increased PGC1α levels. We observed elevation in the protein levels of HSP60, which was already higher in mKO mice, suggesting a contribution of ISR^{mt}, the mammalian counterpart of mitochondrial unfolded protein response, due to possible aggregation of misfolded proteins in mKO animals Figure 5.12b. The protein levels of NRF2 and transcript levels of *Pgc1α* were detected lower in mKOs, but KD treatment did not affect their levels Figure 5.12a and b. A higher amount of TFAM and mitochondrial transcript *Cox1* were unaltered under KD intervention Figure 5.12a and c. We did not detect a difference in VDAC amount in CD or KD-fed mKOs compared to CD-fed WT mice Figure 5.12a.

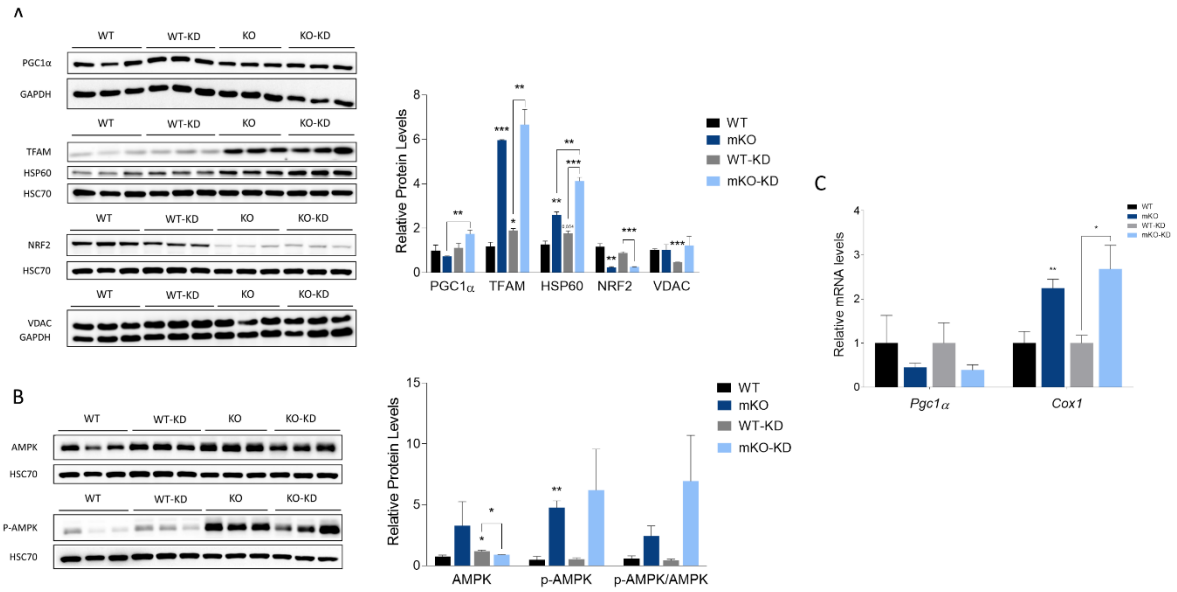

Figure 5.12. The Western Blot analysis (left) and the relative amount (right) of (a) PGC1α, TFAM, HSP60, NRF2, and VDAC, (b) AMPK, p-AMPK (n=3). (c) Quantification of mRNA levels of *Pgc1α* and *Cox1* (n=5). Error bars represent mean ± SEM. Asterisks represent the statistical significance of p values. (Student's t-test: *p<0.05, **p<0.01, ***p<0.001).

Next, we investigated the effect of KD treatment on ISR^{mt} in WT and mKO mice. During ISR^{mt}, eIF2α is inhibited by phosphorylation, which results in attenuation of cytoplasmic translation. On the other hand, CHOP translation is induced by eIF2α phosphorylation to regulate the synthesis of amino acids and antioxidants. Treatment with KD further enhanced the phosphorylation of eIF2α in mKO mice, however, did not significantly affect WT mice but slightly increased the ratio Figure 5.13a. Interestingly, the transcript level of *Chop* was not different in CD and KF-fed control animals, yet the increased *Chop* transcript levels in mKOs were significantly lowered after the intervention Figure 5.13c. For a definitive result, further examination is required on CHOP protein levels. An increase in the protein level of PYCR1 and transcript levels of *Aldh18a1* indicated upregulation of proline synthesis in mKO mice. After KD treatment, we observed further increased *Aldh18a1* levels and slightly increased PYCR1 protein amount Figure 5.13b and c. We detected that the mRNA levels of *Nrf2* were recovered in mKOs due to KD treatment, which was not mirrored in protein levels Figure 5.12a and 13c. Moreover, KD intervention

lowered the strong upregulation of *Mthfd2* and *Fgf21* transcripts in mKOs, but *Gdf15* levels remained unchanged. The levels of ISRmt, mitochondrial folate cycle, and mitokine-related transcripts were not affected by KD treatment in WT animals Figure 5.13c.

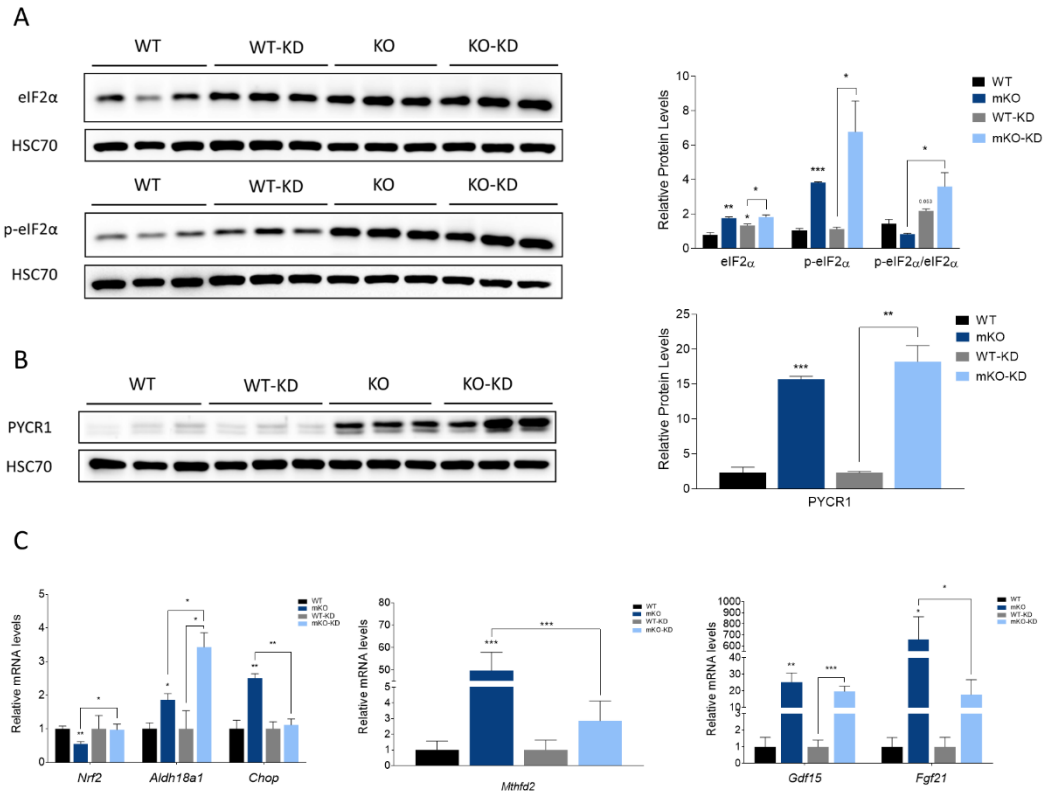

Figure 5.13. The Western Blot analysis (left) and the relative amount (right) of (a) eIF2α and p-eIF2α, (b) PYCR1 (n=3). (c) Quantification of mRNA levels of *Nrf2*, *Ald18a1*, *Chop*, *Mthfd2*, *Gdf15*, and *Fgf21* (n=3-5). Error bars represent mean ± SEM. Asterisks represent the statistical significance of p values. (Student's t-test: *p<0.05, **p<0.01, ***p<0.001).

Mitochondrial dysfunction is usually accompanied by an increase in ROS production; hence upregulation of antioxidant response is expected (Dogan et al., 2014). KD treatment has previously been shown to decrease ROS levels and activate antioxidant response through the upregulation of NFE2L2 (Milder & Patel, 2012). Therefore, we investigated the levels of mitochondrial antioxidant response-associated proteins and transcript. A trend towards decreasing antioxidant response-related transcripts, including *Sod2*, *Catalase*, and *Gpx1*, was observed, reflecting lower *Nfe2l2* levels in mKOs Figure

5.14b. After KD treatment, a slight, albeit insignificant, increase in SOD2 levels was observed in mKOs Figure 5.14a. Interestingly *Sod2* transcript levels did not differ between mKO groups after the treatment but were lower than the controls. The transcript levels of *Sod1* and *Catalase* did not differ significantly, whereas decreased *Gpx1* and *Nfe2l2* levels in mKO mice were increased with KD treatment Figure 5.14b.

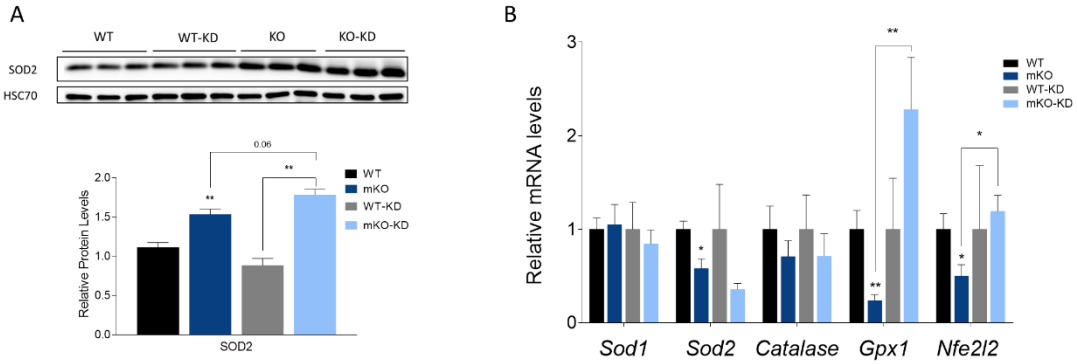

Figure 5.14. The Western Blot analysis (top) and the relative amount (bottom) of (a) SOD2 in CD or KD-fed mice (n=3). (b) Quantification of mRNA levels of *Sod1, Sod2, Catalase, Gpx1,* and *Nfe2l2* (n=3-5). Error bars represent mean ± SEM. Asterisks represent the statistical significance of p values, comparing each group to their relative controls as indicated in the graph. (Student's t-test: *p<0.05, **p<0.01, ***p<0.001).

To test whether KD treatment resulted in a metabolic shift towards β-oxidation, we examined the expression of mRNAs associated with fat metabolism. No difference was detected between CD and KD fed-WT mice, probably due to the short-term of the study. First, we checked the transcript levels of *Fatp1* and *Cd36*, which are required for the import of fatty acids into the cell; while there was no change observed in *Cd36* levels in mKOs, reduced *Fatp1* levels were further decreased in KD-treated mKO mice. ACOX catalyzes the first reaction of β-oxidation in peroxisomes, the desaturation of acyl-CoA, and recovered *Acox* levels in mKOs after KD intervention, indicating activation of peroxisomal β-oxidation. However, we also observed, due to diet change, further reduction in transcript levels of *Cpt1b*, which transfers FAs from the cytoplasm to mitochondria, *Fabp-pm*, a fatty acid binding protein in skeletal muscle, coordinates lipid transport, and *Pdk4*, which decreases glucose utilization and regulate β-oxidation through pyruvate dehydrogenase

inhibition, possibly representing cells reliance on glycolysis during mitochondrial dysfunction. *Pparα* transcripts were similar in all CD or KD-fed test groups. *Ucp3* level is correlated with fatty acid metabolism due to its role in exporting remaining unoxidized fatty acids from mitochondria to prevent accumulation. The decrease in *Ucp3* levels in CD-fed mKOs supports carbohydrate utilization as a primary energy source in their skeletal muscle cells, which was ameliorated in KD-fed mKO mice. The transcript levels of enzymes inducing fatty acid biosynthesis, *Fasn*, and *Srebp1a*, were lower in mKO, *Fasn* levels were increased with KD treatment, yet *Srebp1a* levels did not differ significantly Figure 5.15.

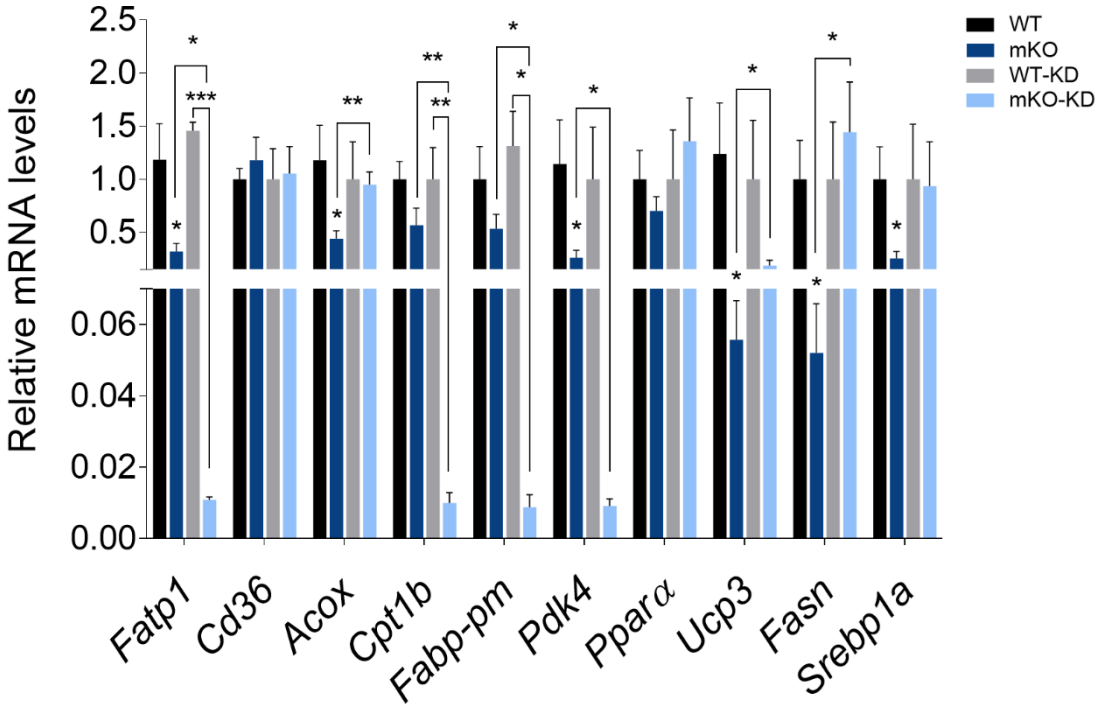

Figure 5.15. The Quantification of lipid metabolism-related mRNA levels of *Fatp1, Cd36, Acox, Cpt1b, Fabp-pm, Pdk4, Pparα, Ucp3, Fasn,* and *Srebp1a* (n=3-5). Error bars represent mean ± SEM. Asterisks represent the statistical significance of p values, comparing each group to their relative controls as indicated in the graph. (Student's t-test: *p<0.05, **p<0.01, ***p<0.001).

We analyzed the amount of P62, which carries ubiquitinated cargo for autophagosomes, and LC3-II, a marker for autophagosome number. A slight increase in P62

levels was observed in mKO and KD-fed WT animals compared to WT mice, indicating stalled autophagy and/or accumulation of ubiquitinylated proteins Figure 5.16b. The ratio of LC3-II was clearly increased in mKO groups, pointing to an increase in the number of autophagosomes and possibly an impairment in their clearance. We observed an insignificant change in the P62 levels, whereas LC3-II levels were on their way to normalization in KD-fed mKO mice Figure 5.16a and b. Especially LC3-II levels might indicate a possible activation of autophagy after KD treatment; however, further experiments are needed to conclude this result definitively.

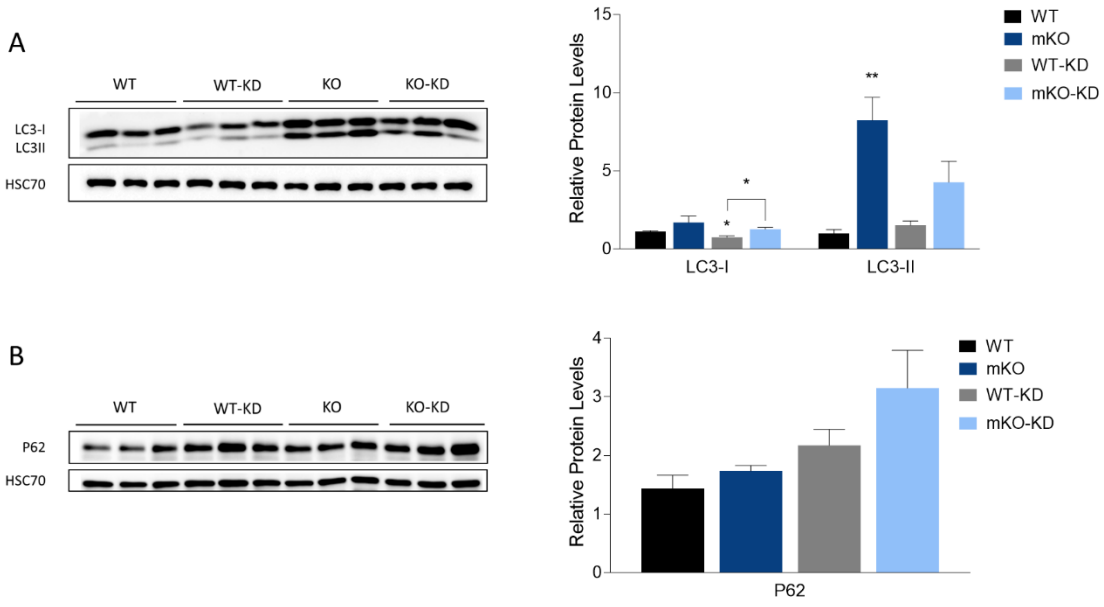

Figure 5.16. The analysis of Western Blot and protein quantification of autophagy markers, (a) LC3-I, LC3-II and (b) P62 of CD or KD-fed mice (n=3). Error bars represent mean ± SEM. Asterisks represent the statistical significance of p values, comparing each group to their relative controls as indicated in the graph. (Student's t-test: *p<0.05, **p<0.01, ***p<0.001).

5.6. AICAR Injection

To the second experimental mice group, AICAR or vehicle (saline as control) were subcutaneously injected in daily doses of 0.5 mg/day/gm of body weight after weaning until mice had to be sacrificed.

5.6.1. Effects of AICAR on Phenotype

The lifespan analysis of the AICAR treatment study group revealed that the AICAR injections did not affect the lifespan of mKOs. The body weight and exercise capability of animals were monitored weekly, and no difference in the body weight of AICAR-injected mice was detected compared to their controls. We detected an insignificant increase in voluntary movements in AICAR-treated WT mice, whereas an insignificant decrease in AICAR-injected mKO mice compared with their respective controls. Interestingly, the motor coordination and balancing abilities of AICAR-injected mKOs were significantly reduced in the 5th and 6th weeks of the experiment; however, the difference was diminished in the 7th week Figure 5.17.

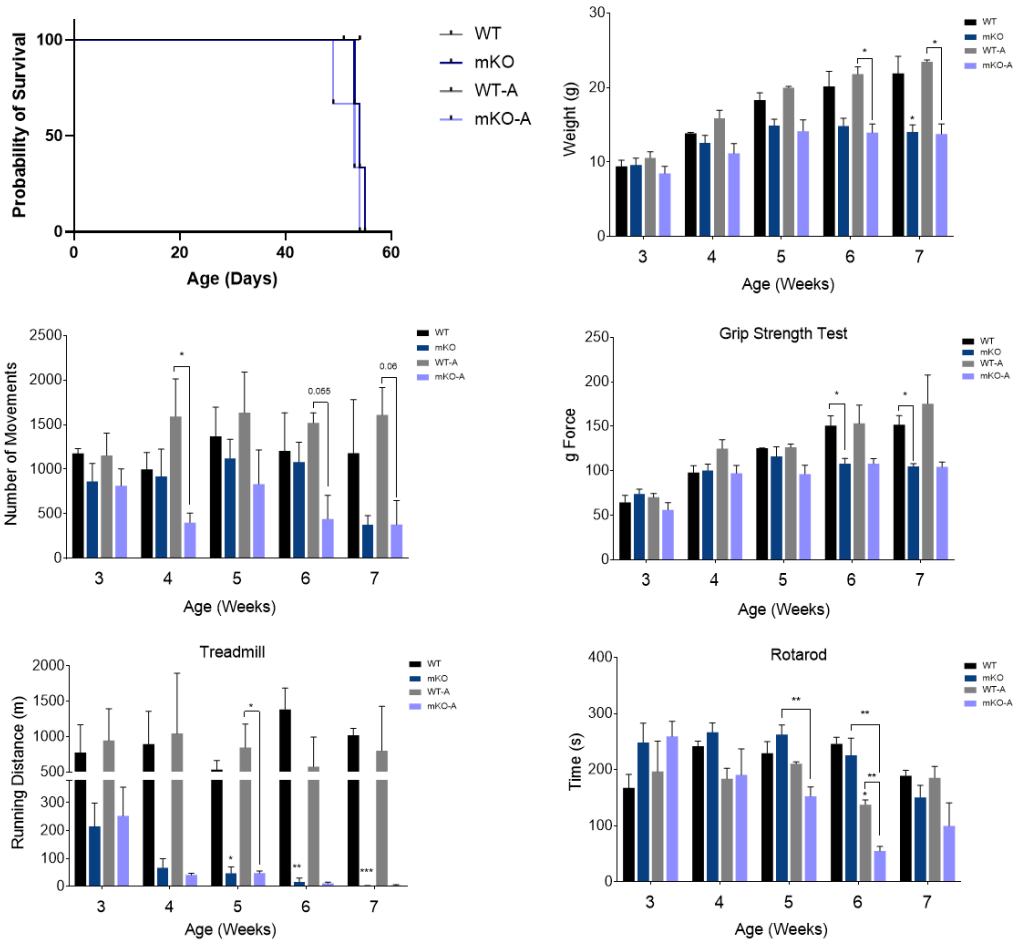

Figure 5.17. Survival curve of AICAR or vehicle WT and skeletal muscle-specific DARS2 KO mouse model (n=2-3). Results of Phenotypic Assays; Weight, Activity Cage (horizontal), Treadmill, Rotarod (n=2-3). Error bars represent mean ± SEM. (Student's t-test: *p<0.05, **p<0.01, ***p<0.001).

5.6.2. Effects of AICAR on Skeletal Muscle Histology

The morphological analysis of skeletal sections of AICAR-treated animals with H&E staining revealed that AICAR injections resulted in an insignificant increase in the cross-sectional area of WT myofibers while a significant increase in mKO myofibers. We observed that the fiber size distribution of AICAR-treated mKO gastrocnemius muscles was not homogeneous, containing a high amount of small, round myofibers and some very large, lighter-in-color myofibers, which might be an indication of repeated cycles of regeneration and degeneration. Moreover, we detected a higher number of smaller myofibers in AICAR-injected WT skeletal muscles. The regeneration process can be examined by detecting myofibers with central nuclei. However, no centralized nuclei were detected in AICAR treatment groups. Further examination of skeletal muscle morphologies of younger mice under AICAR treatment is needed Figure 5.18a and b.

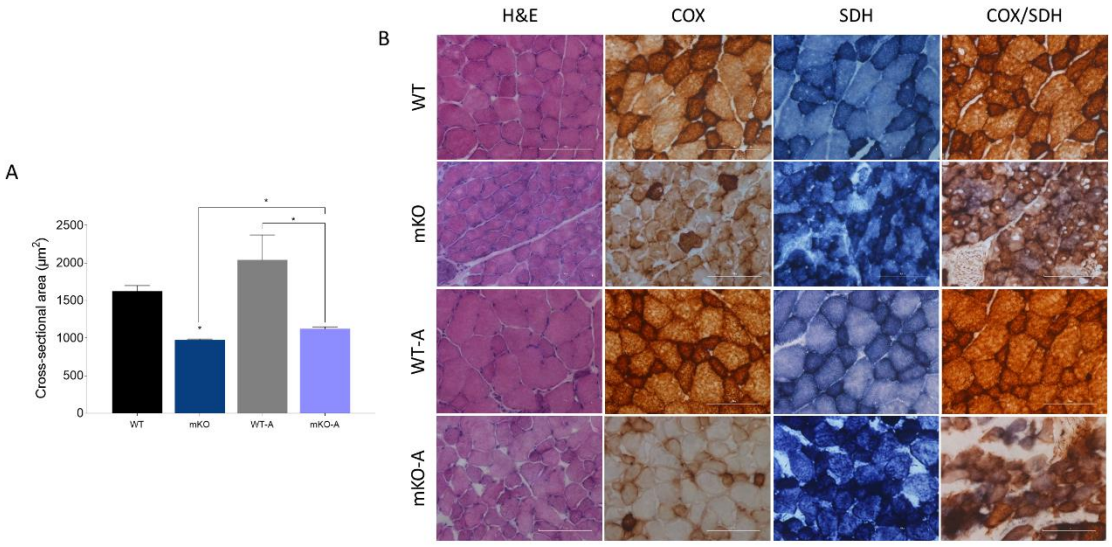

Figure 5.18. Histological and histochemical analysis of AICAR or vehicle WT and mKO muscle fibers (n=2-3). (a) Analysis of the cross-sectional area of skeletal muscle fibers. (b) Histochemical analyses of Hematoxylin and Eosin, COX, SDH, and COX/SDH stainings of skeletal muscle sections of 6–7-week-old WT and mKO animals. Error bars represent mean ± SEM. (Student's t-test: *p<0.05, **p<0.01, ***p<0.001).

The histochemical COX/SDH staining analysis revealed higher COX activity in myofibers of AICAR-treated WT mice; however, no difference in SDH staining was observed. Interestingly, AICAR-treated mKO myofibers exhibited lighter COX precipitation than their controls, indicating defective COX activity. We observed intense precipitation of SDH staining in smaller myofibers of AICAR-injected mKOs, whereas bigger myofibers had detectable lighter staining. The COX/SDH double staining displayed segmentation of blue precipitant in AICAR-treated mKOs, similar to their controls, indicating the transition to RC deficient myofibers Figure 5.18b.

5.6.3. Effects of AICAR on the Molecular Level

The blood glucose levels of the vehicle and AICAR-injected mice were examined weekly. No difference in blood sugar levels was detected in WT mice due to the AICAR injection. However, a significant reduction was observed in blood glucose levels in 4 weeks-old AICAR treated mKOs. The difference did not proceed in the 5th and 6th weeks, yet in the 7th week, an insignificant decrease in blood sugar levels was observed. AICAR treatment might further progress hypoglycemia, and additional examination of blood glucose levels of more mice with AICAR treatment is needed Figure 5.19.

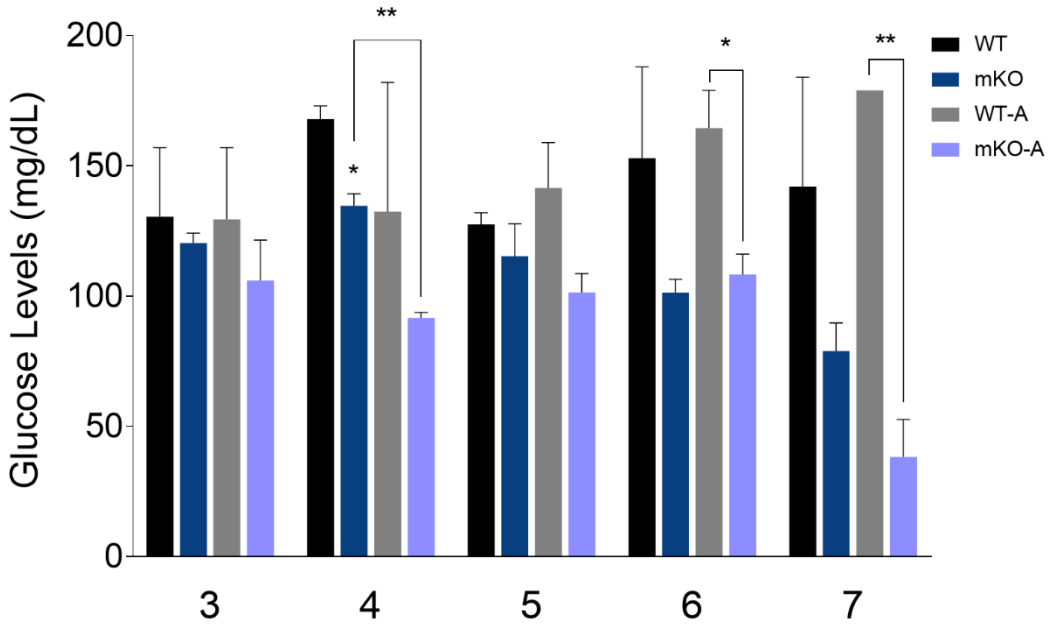

Figure 5.19. The blood glucose levels of AICAR or vehicle-treated mice (n=2-3). Error bars represent mean ± SEM. (Student's t-test: *p<0.05, **p<0.01, ***p<0.001).

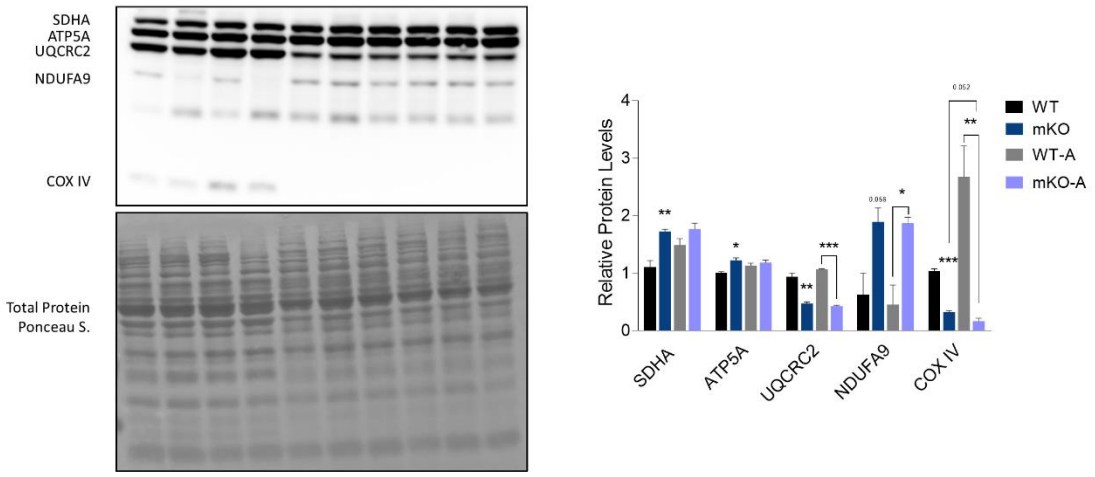

Figure 5.20. The Western Blot analysis (left) and the relative amount (right) of respiratory chain complexes I (NDUFA9-36kDa), II (SDHA-70kDa), III (UQCRC2-45kDa), IV (COX IV-15kDa) and V (ATP5A-55kDa) of the vehicle or AICAR-treated mice (n=2-3). Error bars represent mean ± SEM. Asterisks represent the statistical significance of p values. (Student's t-test: *p<0.05, **p<0.01, ***p<0.001).

The analysis of protein amounts of RC subunits in the skeletal muscle of vehicle or AICAR-injected WT mice showed an insignificant increase in SDHA and COX IV levels. The difference was higher in the amount of COX IV, which we previously observed in the histochemical analysis of COX activity. However, no difference was observed in complexes I, III, and V. AICAR treatment on mKO mice almost significantly (p=0.052) downregulated the amount of COX IV, previously detected in COX staining. Yet, the levels of other RC subunits were unchanged. These results indicated that AICAR treatment did not significantly influence the RC subunit amounts Figure 5.20.

To explore the functional effects of AICAR treatment on mitochondrial biogenesis, associated protein and transcript levels were analyzed. No significant change was observed in AMPK activity in WT and mKO AICAR intervention groups compared to their relative controls, consistent with unaltered protein levels of NRF2 Figure 5.21a and b. Although not significant, the tendency towards an increase in the level of *Pgc1α* in mKOs was recovered by AICAR treatment Figure 5.21c. Similarly, the amount of TFAM, VDAC, and HSP60 remained unchanged, indicating the number of mtDNA and mitochondria did not differ, and

stress response against unfolded proteins was not activated after AICAR treatment Figure 5.21a. An insignificant increase was detected in mtDNA transcript *Cox1* levels in the skeletal muscle of AICAR-injected mice, which could be reflecting an increased number of ribosomes in mitochondria due to the treatment Figure 5.21c.

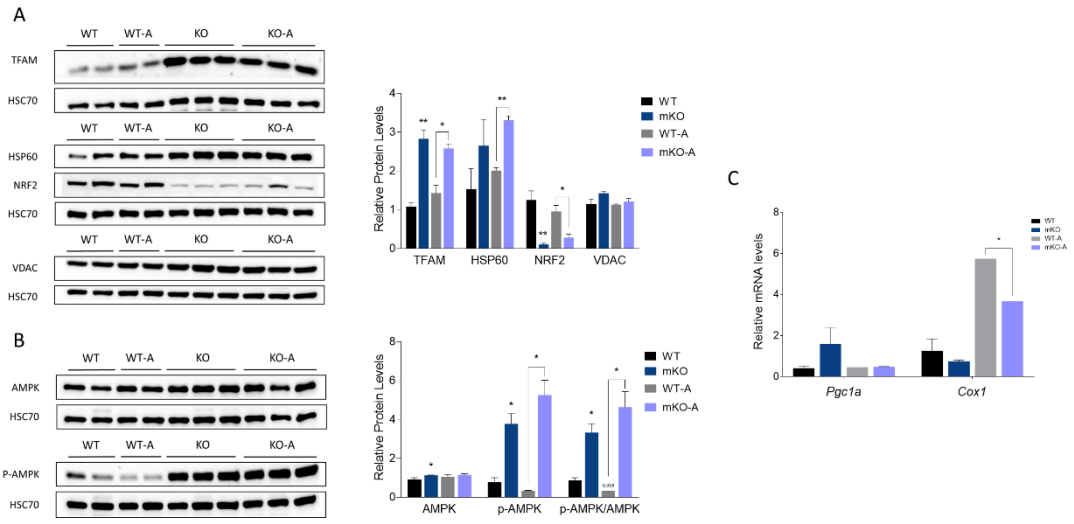

Figure 5.21. The Western Blot analysis (left) and the relative amount (right) of (a) TFAM, HSP60, NRF2, and VDAC, (b) AMPK, p-AMPK, normalized to HSC70 (n=2-3). (c) Quantification of mRNA levels of *Pgc1α* and *Cox1* (n=1-2). Error bars represent mean ± SEM. Asterisks represent the statistical significance of p values (Student's t-test: *p<0.05, **p<0.01).

To study the effects of AICAR on ISR^{mt} induction, we examined related protein and transcript levels. In mKO mice, AICAR injection did not cause a significant change in the protein levels eIF2α and its phosphorylated version, yet it resulted in a significant decrease in the amount of PYCR1, along with lower *Nrf2* and *Chop* transcript levels compared to their vehicle-injected controls, similar to WT animals Figure 5.22. No change was observed in *Aldh18a1* and *Gdf15* levels. The upregulation of Mthfd2 was recovered in AICAR-injected mKO mice. Fgf21 levels, on the other hand, were further elevated in AICAR-treated mKO animals Figure 5.22c.

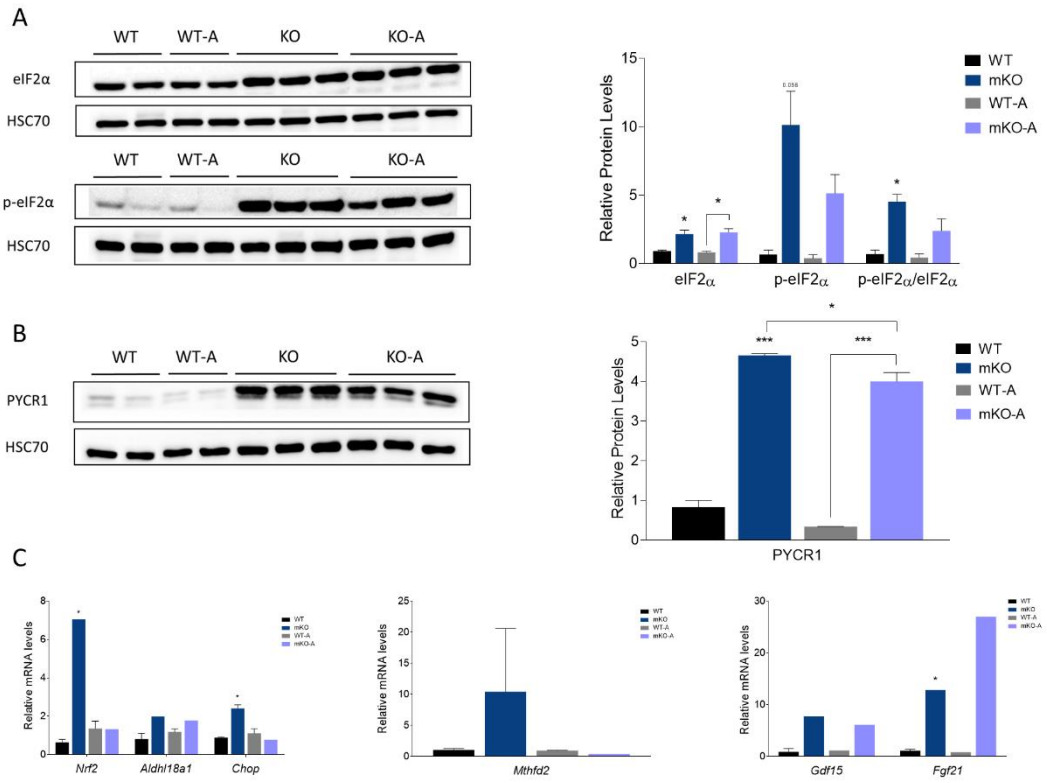

Figure 5.22. The Western Blot analysis (left) and the relative amount (right) of (a) eIF2α and p-eIF2α, (b) PYCR1 (n=2-3). (c) Quantification of mRNA levels of *Nrf2, Ald18a1, Chop, Mthfd2, Gdf15,* and *Fgf21* (n=1-2). Error bars represent mean ± SEM. Asterisks represent the statistical significance of p values, comparing each group to their relative controls as indicated in the graph. (Student's t-test: *p<0.05, **p<0.01, ***p<0.001).

The analysis of antioxidant response-related proteins and transcripts indicated that AICAR treatment did not cause a significant difference in the induction of antioxidant response between vehicle or AICAR-injected test groups, except for the low *Sod1* transcript levels observed in AICAR-treated mKO mice. However, due to the low number of mice administered for this test group, further examinations are necessary to make certain conclusions Figure 5.23.

To understand the possible effect of AICAR treatment on metabolism, we observed the changes on the transcript levels of *Ucp3, Pparα*, and *Pparγ*. We observed a slight decrease in *Ucp3* levels in AICAR-injected mKOs. Moreover, the changes in the transcript levels of *Pparα* and *Pparγ*, which regulates energy metabolism and promotes mitochondrial β-oxidation, reflected the *Pgc1α* levels, a coactivator of *Ppar*s, were increased in mKO mice

and recovered by AICAR treatment (Viscomi et al., 2011). Overall, the analysis of transcript levels suggests a trend of less fat utilization during energy production Figure 5.24.

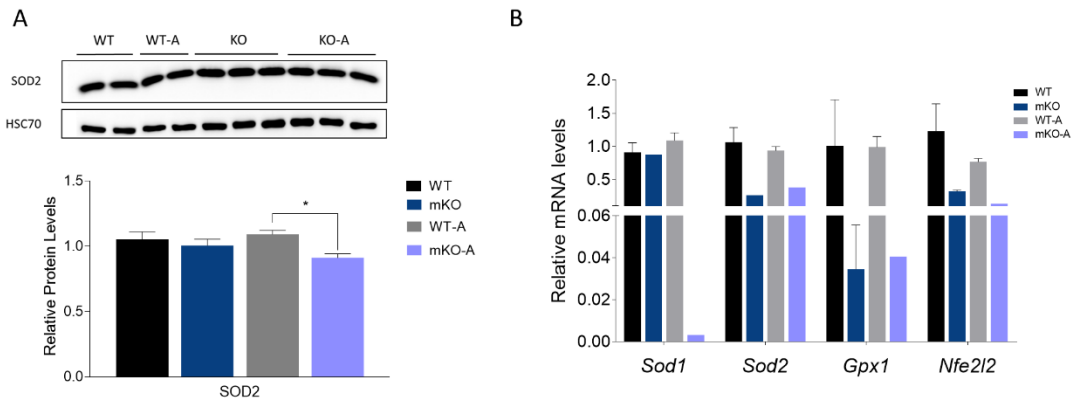

Figure 5.23. The Western Blot analysis (top) of the vehicle or AICAR-treated mice and their relative amount (bottom) of (a) SOD2 normalized to HSC70 (n=2-3). (b) Quantification of mRNA levels of *Sod1*, *Sod2*, *Catalase*, *Gpx1*, and *Nfe2l2* (n=1-2). Error bars represent mean ± SEM. Asterisks represent the statistical significance of p values (Student's t-test: *p<0.05, **p<0.01, ***p<0.001).

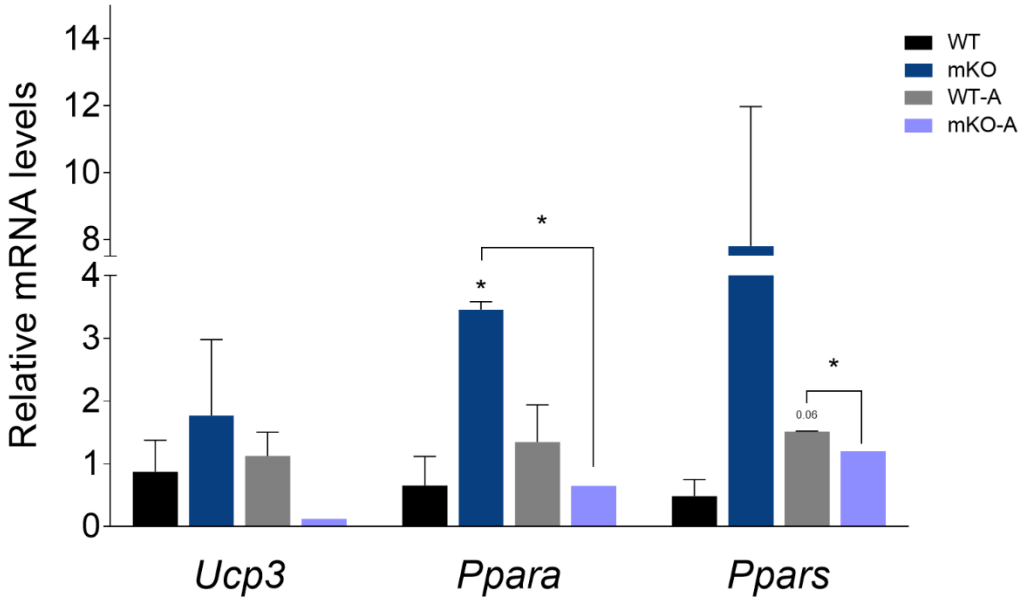

Figure 5.24. The Quantification of lipid metabolism-related mRNA levels of *Ucp3, Pparα,* and *Pparγ* (n=1-2). Error bars represent mean ± SEM. Asterisks represent the statistical significance of p values, comparing each group to their relative controls as indicated in the graph. (Student's t-test: *p<0.05, **p<0.01, ***p<0.001).

The analysis of P62 amounts in the skeletal muscle of vehicle or AICAR-injected animals revealed that AICAR treatment did not alter P62 levels in WTs, however clearly decreased in mKO mice compared to their vehicle-injected controls, indicating clearance of ubiquitinated protein aggregates Figure 5.25.

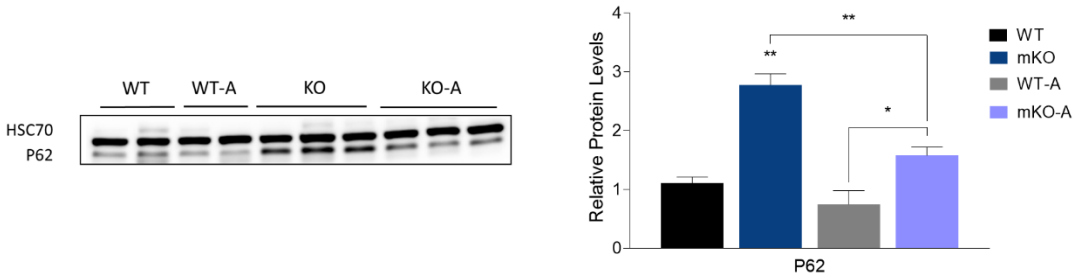

Figure 5.25. The analysis of Western Blot and protein quantification of autophagy marker P62 in the vehicle or AICAR-injected mice (n=2-3). Error bars represent mean ± SEM. Asterisks represent the statistical significance of p values, comparing each group to their relative controls as indicated in the graph. (Student's t-test: *p<0.05, **p<0.01, ***p<0.001).

6. **DISCUSSION AND FUTURE PERSPECTIVES**

Mitochondria are the cell's power plants, producing energy by oxidatively degrading nutrients. Apart from energy production, mitochondria are an integral part of essential metabolic processes, including cell signaling, amino acid biosynthesis, and adapting or reacting to stress conditions; hence defects in mitochondrial dynamics can elicit a broad range of disorders, from age-related diseases to cancer. Mitochondrial disorders are challenging to diagnose as their manifestation is highly dependent on mitochondrial heterogeneity. They may affect any tissue at any age, especially tissues highly reliant on energy, such as skeletal muscles. Many mitochondrial diseases are incurable; therefore, mechanisms behind mitochondrial dysfunction still need to be unveiled, and is crucial to develop effective treatment methods against disease symptoms.

This thesis brings a new perspective to mitochondrial disease research area in two aspects; understanding tissue-specific responses to mitochondrial dysfunction and their management. Our first aim was to further characterize and understand the skeletal muscle-specific manifestation of mitochondrial translation deficiency in a DARS2-depleted mouse model (mKO). We proceeded with trials of alleviating disease progression with potential supportive treatment methods.

The DARS2 mKO was previously generated and preliminarily studied by our lab. Ablation of *Dars2* in skeletal muscle by Cre recombinase under expression of the human-alpha skeletal actin 1 (ACTA1) promoter led to premature death by around 7 weeks of age due to mitochondrial translation defects and OXPHOS deficiency. In contrast, heterozygous mice did not exhibit any characteristics of the mouse model, pointing to one copy of the gene is sufficient to maintain the synthesis of mtDNA-encoded proteins.

Due to the severe early-onset mitochondrial myopathy progression, the mouse model exhibited lower physical performance, weaker muscle strength, and rapid muscle fatigue with decreased body weight and gastrocnemius size. The mouse model also progressively developed hypoglycemia. Lowered blood glucose levels might indicate that glucose was utilized by the skeletal muscle cells for energy production through glycolysis. As the

compensatory mechanism against RC deficiency, characterized by the reduction in OXPHOS complex levels, mitochondrial biogenesis, antioxidant response, and ISR^{mt} were induced in the skeletal muscle of mKO along with impaired autophagy (Yılmaz, 2022). Skeletal muscle atrophy and fiber loss have been associated with mitochondrial dysfunction and myopathy. Increased atrophy marker levels in mKO mice observed previously in a study (Yılmaz, 2022), yet immunohistochemical analysis was lacking. The morphological analysis of skeletal muscle cross-sections revealed that KO myofibers were smaller due to atrophy, indicating exercise intolerance in the mouse model. The prevalence of COX-deficient myofibers with high SDH activation in mKO mice is a clear sign of mitochondrial myopathy, yet with the presence of segmental COX/SDH accumulation, representing an incomplete transition from normal to respiratory deficient fibers. Examining the transition between fiber status can be a supportive measure to evaluate the effects of treatments on disease progression (Murphy et al., 2012). Similar to skeletal muscle-specific loss of DARS2, the mitochondrial translation deficiency mouse models, *Pus1*, *Lrpprc*, and *Tfb1m* KO mouse models displayed strong COX deficiency in muscle or cardiac cells. Moreover, SDH activity did not differ from *Tfb1m* KO mice, whereas *Pus1* KO mice showed decreased SDH precipitation and increased cross-sectional area of myofibers without centrally localized nuclei (Metodiev et al., 2009; Magnum et al., 2016; Mourier et al., 2014).

ROS are by-products mainly generated from at least 11 distinct sites of ETC during oxidative respiration (Wong et al., 2017; Goncalves et al., 2020). Fluctuation in ROS levels is theorized participate in metabolic homeostasis as a signaling molecule; increased levels of ROS production due to dysfunctional RC are deleterious and can harm cellular compartments, while reduced ROS levels regulate mitochondrial energy-producing pathways, facilitating adaptation to stress conditions (Scialò et al., 2017; Yun & Finkel, 2014). ROS is produced in a high ratio from CI, particularly during RET or inhibition of CIII and/or CIV. Mammalians have developed a compensatory mechanism to cope with elevated ROS levels, called antioxidant response (Dogan et al., 2018; Scialò et al., 2017; Yun & Finkel, 2014). ROS production during FET was significantly higher in mKO mice compared to their controls when mitochondria were supplemented with CI substrate. The inhibition of CIII with antimycin A resulted in reduced ROS levels. ROS production was lower in mKO mice during RET, and further reduction was observed in the presence of the CI inhibitor. We reasoned that ROS is mainly produced from CI during FET in the skeletal muscle of DARS2-

depleted mice. Heart-specific DARS2 depletion resulted in decreased oxygen consumption accompanied by reduced ATP production and ROS generation during RET, yet no difference in ROS levels during FET was detected (Kartal, 2022). Conversely, the loss of *Lrpprc* led to increased ROS production (Mourier et al., 2014). Depending on stress conditions and substrate combinations, site-specific ROS generation can affect the activity of specific proteins by changing their redox state (Scialò et al., 2017). Thus, the amount of ROS produced from different complex sites could signal to activate specific pathways and stress responses and have a therapeutic effect. Site-specific suppression of ROS production via small targeting molecules, such as S1QELs, S3QELs, and NOX inhibitors, without influencing OXPHOS may help us understand the relative contribution of site-specific ROS production and the amount in the activation of different stress responses (Wong et al., 2017; Goncalves et al., 2020).

The oxygen consumption rate represents ATP production capacity and the production of ROS during OXPHOS, which is used to assess mitochondrial integrity (Hartman et al., 2014). The reduced OCR in mKO muscle is not consistent with ROS production during FET when supplemented with pyruvate and malate, indicating oxygen utilization was based on ROS generation rather than energy production. Furthermore, the overall OCRs were significantly lowered during both CI and CII-linked respiration, supporting loss of OXPHOS activity due to RC deficiency in the skeletal muscle of mKO mice. *Lrpprc* KO mice displayed a reduced respiratory rate during state 3 respiration and lower ATP production (Mourier et al., 2014). On the contrary, *Wars2* mutant mouse embryonic fibroblasts (MEFs) exhibited higher basal respiration and energy production than wild-type MEFs, indicating increased OXPHOS (Agnew et al., 2018).

The mitochondrial membrane potential generated from proton transfer across the inner membrane is essential for energy production and is used as a measure of mitochondrial function (Zorova et al., 2018). Like increased ROS production, loss of mitochondrial membrane potential is observed under stress conditions and mitochondrial dysfunction (Suski et al., 2012). Unlike ROS, which can diffuse and travel far from mitochondria as a signaling molecule, the change in mitochondrial membrane potential cannot be emitted (Scialò et al., 2017). The mitochondrial membrane potential was elevated in mKO muscles when supplemented with CI substrates, indicating generation of the electrochemical gradient

is not the main reason behind the severe phenotype of the mouse model (Dogan et al., 2018; Scialò et al., 2017; Yun & Finkel, 2014). Heart-specific DARS2 depletion did not result in a difference in mitochondrial membrane potential, whereas the *Lrpprc*-depleted mouse model was not able to maintain membrane potential during state 3 respiration (Mourier et al., 2014). The variety of responses to mitochondrial translation deficiency in different mouse models suggests that mitochondrial dysfunctions are cell and disease-type specific, and should be managed with separate treatments.

Even though mitochondrial dysfunction is common and part of many disorders, effective treatments against disease progression are still unavailable. Here, we studied the effects of KD intervention and daily AICAR injection on the severe early-onset mitochondrial mouse model, which have previously been shown to be effective in slowing mitochondrial myopathy progression.

Under a regular carbohydrate-rich diet, skeletal muscle cells with mitochondrial dysfunction shift their metabolism towards glycolysis, in order to not utilize their mitochondria. Under low carbohydrate, high lipid diet intervention, cells are compelled to use their mitochondria as lipids can only be converted into energy through β-oxidation in mitochondria (Ahola et al., 2016). In theory, cells will need more mitochondrial proteins for energy production, activating mitochondrial biogenesis in response to diet intervention.

KD has been tested as a supportive treatment to reduce epileptic attacks in patients. Seizures were reported to be reduced by diet change, especially in patients with CI deficiency. However, the study groups of human patients are fewer in number (Kang et al., 2007). The late-onset progressive mitochondrial myopathy mouse model, named Deletor after accumulation of mtDNA deletion due to overexpression of mutant Twinkle, was treated with KD and exhibited decelerated disease progression, induced mitochondrial biogenesis, reduced COX-deficient fibers, and improved metabolic parameters as a result. The study shows the beneficial act of stimulating mitochondrial biogenesis in mild RC deficiency cases and that RC deficiency can be compensated by inducing OXPHOS through diet intervention (Ahola-Erkkilä et al., 2010). On the other hand, a previous study on an astrocyte-specific KO mouse model for TWINKLE revealed aggregated brain pathology progression after KD treatment and caused early termination of the trial (Ignatenko et al., 2020). The skeletal

muscle of PEO patients also showed an inability to shift their metabolism to β-oxidation under mAD treatment. Their ragged red fibers, highly dependent on glycolysis, were affected the most (Ahola et al., 2016). However, whether mitochondrial biogenesis induction through KD will be effective in severe mitochondrial myopathy mouse models with early-onset disease progression has remained unanswered.

The very first consequence of KD intervention that was observed on mKO mice was a further shortened lifespan. However, the behavioral test group of KD-fed mKOs lived longer than the lifespan cohort, although CD and KD-fed mKO study groups displayed similar exercise capacity. As also seen in mKO mice, exercise intolerance is associated with mitochondrial dysfunction. Even though the effects of exercise treatment are still under debate, various studies showed that exercise training could improve a patient's quality of life and attenuate muscle atrophy. Exercise-based therapy consists of two types of training: endurance and resistance. Endurance exercises refer to long-term walking, running, and swimming, while resistance exercises refer to activities that increase muscle strength. Resistance exercise has been shown to induce mitochondrial biogenesis and increase oxidative capacity in patients (Taivassalo et al., 1999). Mouse studies with endurance exercises have also shown beneficial effects, such as improving oxygen utilization and exercise tolerance. Under long-term exercise training, a mouse with a POLG defect exhibited recovered mitochondrial morphology and OXPHOS capacity (Safdar et al., 2011). The Harlequin mouse model with CI deficiency also showed improved muscle strength and atrophy after endurance training (Fiuza-Luces et al., 2019). However, whether endurance exercise affected the pathogenesis or solely attenuated deconditioning in KD-fed mKOs needs further research.

The significant increase in the ratio of gastrocnemius muscle to body without an improved cross-section area of myofibers in KD-treated mKO mice suggests an increase in myofiber number. Histochemical analysis of skeletal muscle revealed darker COX staining and more homogeneous precipitation of SDH. We concluded that the rise in the number of myofibers might not be a result of regeneration but due to halted turnover of more mature myofibers, which have complete RC deficiency.

Previous results from our lab revealed that DARS2 depletion in skeletal muscle exhibited downregulation in CI, CIII, and CIV subunits, while upregulation in CII and CV (Yılmaz. 2022). Our results confirmed these observations, apart from CI values, which were also insignificantly upregulated in mKO muscles. To achieve specific data on CI subunit levels, antibodies specific to individual complexes must be used rather than a complex cocktail. The elevated CI values were also supported by data on increased oxygen consumption and ROS production under CI substrate supplementation. This is explained by the higher number of nuclear-encoded subunits of CI compared to CIII and CIV. Increased CI, CII, and CV levels in mKO might be related to mitochondrial biogenesis induction. Furthermore, KD intervention in control mice caused a slight, albeit insignificant, increase in CI, CIII, and CIV levels, suggesting upregulation in the protein levels containing mitochondrial encoded subunits. KD-treated control mice in another study have also been shown to have higher mtDNA numbers, which was also confirmed by elevated TFAM levels in KD-fed WTs (Ahola et al., 2016). However, these results were not mirrored in KD-fed mKOs. Thus, the decline in the upregulation of RC with mtDNA-encoded subunits with elevation in CII expression in mKOs under KD intervention supports the severity of the phenotype of the mouse model and that KD intervention is not efficient enough to attenuate the effects of mitochondrial translation deficiency in a mere 4 weeks. The effects of KD intervention could be more pronounced if the trial was for a longer duration. In addition to the protein levels RC subunit, the analysis of the complex activities will provide a comprehensive understanding of the effects of mitochondrial translation deficiency.

PGC1α has been shown to ameliorate RC dysfunction in mouse models carrying severe COX deficiency (Wenz et al., 2008; Viscomi et al., 2011). Mitochondrial biogenesis can be induced by PGC1α activation through AMPK (Skrobuk et al., 2012; Lagouge et al., 2006). Elevated AMPK phosphorylation was not reflected in PGC1α and NRF2 levels in mKO. AMPK regulates various metabolic pathways in skeletal muscle, including β-oxidation and glucose transport. Thus, the results indicate that activated AMPK might have a role in lipid and glucose utilization in the skeletal muscle of mKOs rather than inducing mitochondrial biogenesis.

FGF21, a biomarker for mitochondrial myopathy and ISR^{mt}, has previously been shown to be secreted from COX-deficient fibers to convey the rest of the organism about the

metabolic condition of the muscle (Khan et al., 2014). Interestingly, increased *Fgf21* transcript levels in DARS-depleted mice were recovered after KD treatments, albeit higher than in control groups, consistent with the ratio of COX-negative fibers determined by histochemical analysis. The FGF21 levels in the blood serum of test cohorts must be examined to confirm our data on transcript levels and histology. Besides, the cytoplasmic protein, amino acid, and antioxidant synthesis were downregulated in KD-fed mKO animals. The overall decrease in ISR^{mt} components and upregulation in proline biosynthesis might be a sign of improvement in mitochondrial myopathy and cell metabolism (Khan et al., 2017; Kardos et al., 2015). Conversely, KD treatment on mKO activated antioxidant response and upregulated downstream target genes, pointing to potential ROS involvement. Further examination of ROS production, DNA damage, and lipid peroxidation should be employed to understand the reason behind the induction of antioxidants (Dong et al., 2008).

The analysis of fatty acid metabolism-related transcript levels confirmed our expectations of the preference for glucose metabolism in skeletal muscle-specific DARS2-deficient mice due to mitochondrial dysfunction. KD therapy demonstrated further downregulation of the genes associated with fatty acid import and mitochondrial β-oxidation, whereas upregulation in genes involved in the removal of fatty acids from mitochondria, peroxisomal β-oxidation, and fatty acid biosynthesis, promoting lipid storage was observed. This study revealed that during KD intervention, the early-onset mitochondrial myopathy mouse model relies highly on non-oxidative energy production and cannot switch energy metabolic mode to fatty acid utilization.

DARS2 depletion resulted in the accumulation of autophagosomes and impaired their clearance. The treatment with KD rescued the block of autophagic flux while the ubiquitinated protein levels remained high. Under-low nutrient conditions, cells can produce substrate for ATP production and building blocks for protein synthesis via autophagy. The resistance of skeletal muscle to shift their energy production towards β-oxidation might have driven the cells to activate autophagic machinery to produce sugars through the degradation of protein complexes. However, the autophagic marker turnover assay by colchicine injection and monitoring the rate of LC3-II accumulation can further explain autophagy dynamics in the skeletal muscle cells (Ju et al., 2016; Seiliez et al., 2016; Moulis & Vindis, 2017). KD intervention might have induced selective degradation of dysfunctional

mitochondria via autophagy, known as mitophagy, to shift the heterogeneity in the cell towards a healthy state of mitochondria (Feng et al., 2022). Further analysis of the protein levels associated with the elimination of mitochondria by autophagy can help understand the recovery of autophagic flux by KD treatment.

This study reveals that the beneficial effects of KD, including mitochondrial biogenesis induction, boosting RC activity, and overcoming COX deficiency in mild mitochondrial myopathy mouse models, are not mirrored in our early-onset myopathy model. Our results strongly suggest that the type of available nutrient is not sufficient enough in severe myopathy cases to modify energy metabolism and cannot hamper the fatal progression in a mere 4-week trial, highlighting the importance of the generation of mouse models carrying disease phenotypes and mouse trials on promising treatments before initiating on human patients.

In the second study, we examined the effects of pharmacological treatment with AMPK agonist AICAR on skeletal muscle-specific DARS2-depleted mice. The activation of mitochondrial biogenesis by AICAR injection has proven to alleviate mitochondrial myopathy symptoms. Short-term treatment with AICAR revealed partial recovery of COX activity in three myopathy mouse models via increasing AMPK phosphorylation and inducing energy production by β-oxidation, while significantly improving motor performances in one of the mouse models (Viscomi et al., 2011). Similarly, prolonged AICAR treatment improved COX activity and motor performances and induced skeletal muscle regeneration in a mouse model with slow myopathy progression, leading to delayed onset of mitochondrial myopathy (Peralta et al., 2016).

The morphological analysis of DARS2-deficient myofibers exhibited nonhomogeneous fiber size along the muscle. A potential reason for the variety in fiber size is the induction of muscle regeneration, which was also observed in AICAR-treated control mice. Our observations on muscle morphology support previous results on the activation of muscle regeneration by AICAR treatment (Peralta et al., 2016). While previously studied mouse models showed elevated COX activity, mKO mice revealed reduced COX activity accompanied by uneven SDH precipitation, an indication of transition in fiber state (Viscomi et al., 2011; Peralta et al., 2016). AICAR-treated mKO mice showed further induction of

hypoglycemia. The reduction in blood glucose levels might reflect the nutrient need of newly generated myofibers.

Recovery from ISR^{mt} markers has been thought to alleviate myopathy manifestation. Our observation of the decreased levels of ISR^{mt} components correlates with the beneficial effects of the treatment. However, elevated expression of *Fgf21* disaffirmed our observations on the activation of ISR^{mt}. As the FGF21 is secreted from COX-negative fibers to convey to other tissues in the organism, we can conclude that the change in *Fgf21* transcript levels reflected the further reduction in COX activity (Khan et al., 2014). To make a clear conclusion, the blood serums of the mice should be examined for FGF21.

Remarkably, we did not observe a significant difference in the levels of AMPK activation, which was mirrored by general mitochondrial biogenesis markers. Similarly, the expression of the genes associated with the antioxidant response remained unaltered after the treatment. The dosage sensitivity for AICAR injection was observed in previous studies (Viscomi et al., 2011). Even though the AICAR serum concentration (0.5 mg/day/gm) in this study was decided according to the responses from previously studied mouse models, not every mouse model can react to the exact dosage of treatments. The dosage concentration administered to mice with slow progression of myopathy probably did not efficiently affect the severe phenotype of our early-onset myopathy model. The study can be repeated with higher AICAR concentrations to have a broader insight into the beneficial effects of the treatment method.

The increase in fat utilization due to AICAR injection on different mouse models was not carried in DARS2-ablated skeletal muscles. The persistence of glycolytic energy production highlights the severity of the phenotype of mKO mice and the enhanced tendency for glycolysis after the treatment. Further investigation on the level of enzymes responsible for glucose degradation to pyruvate is necessary to support our observations.

The decrease in P62 protein levels indicates two possible outcomes; reduced ubiquitination of proteins or activated clearance of the protein aggregates. The significant difference between AICAR-treated control and mKO cohorts supports the latter. Analyzing autophagy and mitophagy marker levels is necessary to prove the same.

This study provides an essential perspective on mitochondrial disease treatment and management. AICAR treatment, although not sufficient to alleviate myopathic phenotypes, is effective in promoting muscle regeneration without inducing mitochondrial biogenesis.

Skeletal muscle is an adaptive tissue containing different types of myofibers; type I oxidative-slow twitch, and type II glycolytic-fast twitch, glycolytic- and oxidative-fast twitch. These tissues can differentiate and transform into one another when required. The transition from fast to slow-twitch fiber type is associated with enhanced exercise endurance (Peralta et al., 2016). The analysis of the relative expression of fiber-type specific transcripts, such as contractile proteins, will extend our understanding of the effects of treatments on fiber metabolism.

In conclusion, the supportive treatment methods, KD intervention, and AICAR injection, although while improving mitochondrial myopathy through different mechanisms without inducing mitochondrial biogenesis, were not significant enough in alleviating the severe phenotype of the skeletal muscle-specific DARS2-deficient mouse model. It also highlights that mitochondrial myopathy occurs through different pathways in different mouse models. In case of human beings, the heterogeneity and tissue specificity of this disorder depend on the individual. Hence, the promising results of a disease-specific treatment method cannot be generalized over different mitochondrial disorders without adequate experimentation.

REFERENCES

Agnew, T., M. Goldsworthy, C. Aguilar, A. Morgan, M. Simon, H. Hilton, C. Esapa, Y. Wu, H. Cater, L. Bentley, C. Scudamore, J. Poulton, K.J. Morten, K. Thompson, L. He, S.D.M. Brown, R.W. Taylor, M.R. Bowl and R.D. Cox, 2018, "A Wars2 Mutant Mouse Model Displays OXPHOS Deficiencies and Activation of Tissue-Specific Stress Response Pathways", *Cell Reports*, Vol. 25, No. 2, pp. 3315–3328.

Ahola-Erkkilä, S., C.J. Carroll, K. Peltola-Mjösund, V. Tulkki, I. Mattila, T. Seppänen-Laakso, M. Oresic, H. Tyynismaa and A. Suomalainen, 2010, "Ketogenic Diet Slows Down Mitochondrial Myopathy Progression in Mice", *Human Molecular Genetics*, No. 19, Vol. 10, pp. 1974–1984.

Ahola, S., M. Auranen, P. Isohanni, S. Niemisalo, N. Urho, J. Buzkova, V. Velagapudi, N. Lundbom, A. Hakkarainen, T. Muurinen, P. Piirilä, K.H. Pietiläinen and A. Suomalainen, 2016, "Modified Atkins Diet Induces Subacute Selective Ragged-Red-Fiber Lysis in Mitochondrial Myopathy Patients", *EMBO Molecular Medicine*, Vol. 8, No. 11, pp. 1234–1247.

Anderson, S., A.T. Bankier, B.G. Barrell, M.H. de Bruijn, A.R. Coulson, J. Drouin, I.C. Eperon, D.P. Nierlich, B.A. Roe, F. Sanger, P.H. Schreier, A.J. Smith, R. Staden and I.G. Young, 1981, "Sequence and Organization of the Human Mitochondrial Genome", *Nature*, Vol. 290, No. 5806, pp. 457–465.

Ashfaq, M., A.R. Moats, H. Northrup, C.N. Singletary, S.S. Hashmi, M.K. Koenig, M.B. Bagg, and D. Rodriguez-Buritica, 2021, "Hypoglycemia in Mitochondrial Disorders", *Mitochondrion*, Vol. 58, pp. 179–183.

van Berge, L., S. Dooves, C.G.M. van Berkel, E. Polder, M.S. van der Knaap and G.C. Scheper, 2012, "Leukoencephalopathy with Brain Stem and Spinal Cord Involvement and Lactate Elevation is Associated with Cell-type-dependent Splicing of mtAspRS mRNA", *Biochemical Journal*, Vol. 441, No. 3, pp. 955–962.

Bezawork-Geleta, A., J. Rohlena, D. Lanfeng, P. Karel and J. Neuzil, 2017, "Mitochondrial Complex II: At the Crossroads", *In Trends in Biochemical Sciences*, Vol.42, No.4, pp. 312–325.

Birky, C.W., 2001, "The Inheritance of Genes in Mitochondria and Chloroplasts: Laws, Mechanisms, and Models", *Annual Review of Genetics*, Vol. 35, pp. 125–148.

Bough, K.J., J. Wetherington, B. Hassel, J.F. Pare, J.W. Gawryluk, J.G. Greene, R. Shaw, Y. Smith, J.D. Geiger and R.J. Dingledine, 2006, "Mitochondrial Biogenesis in the Anticonvulsant Mechanism of the Ketogenic Diet", *Annals of Neurology*, Vol. 60, No. 2, pp. 223–235.

Cantó, C. and J. Auwerx, 2010, "AMP-Activated Protein Kinase and Its Downstream Transcriptional Pathways", *Cellular and Molecular Life Sciences*, Vol. 67, No. 20, pp. 3407–3423.

Carroll, J., I.M. Fearnley, J.M. Skehel, R.J. Shannon, J. Hirst and J.E. Walker, 2006, "Bovine Complex I is a Complex of 45 Different Subunits", *Journal of Biological Chemistry*, Vol.281, No. 43, pp. 32724-32727.

Cahaban, Y., E.J. Boekema and N.V. Dudkina, 2014, "Structures of Mitochondrial Oxidative Phosphorylation Supercomplexes and Mechanisms for Their Stabilization", *Biochimica et Biophysica Acta - Bioenergetics*, Vol. 1837, No. 4, pp. 418-426.

Cámara, Y., J. Asin-Cayuela, C.B. Park, M.D. Metodiev, Y. Shi, B. Ruzzenente, C. Kukat, B. Habermann, R. Wibom, K. Hultenby, T. Franz, H. Erdjument-Bromage, P. Tempst, B.M. Hallberg, C.M., Gustafsson and N.G. Larsson, 2011, "MTERF4 Regulates Translation by Targeting the Methyltransferase NSUN4 to the Mammalian Mitochondrial Ribosome", *Cell Metabolism*, Vol. 13, No. 5, pp. 527–539.

Dagenais, G.R., R.G. Tancredi and K.L. Zierler 1976, "Free Fatty Acid Oxidation by Forearm Muscle at Rest, and Evidence for an Intramuscular Lipid Pool in the Human Forearm", *Journal of Clinical Investigation*, Vol. 58, pp. 421-431.

Davison, J.E. and S. Rahman, 2017, "Recognition, Investigation and Management of Mitochondrial Disease", *Archives of Disease in Childhood*, Vol. 102, No. 11, pp. 1082–1090.

Dogan, S.A., C. Pujol, P. Maiti, A. Kukat, S. Wang, S. Hermans, K. Senft, R. Wibom, E.I. Rugarli and A. Trifunovic, 2014, "Tissue-Specific Loss of DARS2 Activates Stress Responses Independently of Respiratory Chain Deficiency in the Heart", *Cell Metabolism*, Vol. 19, No. 3, pp. 458–469.

Wong, H.S., P.A. Dighe, V. Mezera, P.A. Monternier and M.D. Brand, 2017, "Production of Superoxide and Hydrogen Peroxide from Specific Mitochondrial Sites Under Different Bioenergetic Conditions", *The Journal of Biological Chemistry*, Vol. 292, No. 41, pp. 16804–16809.

Dong, J., K.K. Sulik and S.Y. Chen, 2008, "Nrf2-Mediated Transcriptional Induction of Antioxidant Response in Mouse Embryos Exposed to Ethanol in Vivo: Implications for the Prevention of Fetal Alcohol Spectrum Disorders", *Antioxidants & Redox Signaling*, Vol. 10, No. 12, pp. 2023–2033.

Falkenberg, M., 2018, "Mitochondrial DNA Replication in Mammalian Cells: Overview of the Pathway", *Essays in Biochemistry*, Vol. 62, No. 3, pp. 287–296.

Feng, Y., J. Xu, M. Shi, R. Liu, L. Zhao, X. Chen, M. Li, Y. Zhao, J. Chen, W. Du and P. Liu, 2022, "COX7A1 Enhances the Sensitivity of Human NSCLC Cells to Cystine Deprivation-Induced Ferroptosis via Regulating Mitochondrial Metabolism", *Cell Death & Disease*, Vol. 13, No. 11, pp. 988.

Fiuza-Luces, C., P.L. Valenzuela, S. Laine-Menéndez, M. Fernández-de la Torre, V. Bermejo-Gómez, L. Rufián-Vázquez, J. Arenas, M.A. Martín, A. Lucia and M. Morán, 2019, "Physical Exercise and Mitochondrial Disease: Insights From a Mouse Model", *Frontiers in Neurology*, Vol. 10, pp. 790.

Frey, T.G. and C.A. Mannella, 2000, "The Internal Structure of Mitochondria", *Trends in Biochemical Sciences*, Vol. 25, No. 7, pp. 319–324.

Giménez-Xavier, P., R. Francisco, F. Platini, R. Pérez and S. Ambrosio, 2008, "LC3-I Conversion to LC3-II Does Not Necessarily Result in Complete Autophagy", *International Journal of Molecular Medicine*, Vol. 22, No. 6, pp. 781–785.

Glick, D., S. Barth and K.F. Macleod, 2010, "Autophagy: Cellular and Molecular Mechanisms", *J Pathol*, Vol. 221, No 1, pp. 3-12.

Goldstein, M.S., V. Mullick, B. Huddlestun and R. Levine, 1953, "Action of Muscular Work on Transfer of Sugars Across Cell Barriers; Comparison with the Action of Insulin", *American Journal of Psychology*, Vol. 173, pp. 212-216.

Goncalves, R.L.S., M.A. Watson, H.S. Wong, A.L. Orr and M.D. Brand, 2020, "The Use of Site-Specific Suppressors to Measure the Relative Contributions of Different Mitochondrial Sites to Skeletal Muscle Superoxide and Hydrogen Peroxide Production", *Redox Biology*, Vol. 28, pp. 101341.

Gureev, A.P. and V.N. Popov, 2019, "Nrf2/ARE Pathway as a Therapeutic Target for the Treatment of Parkinson Diseases", *Neurochemical Research*, Vol. 44, No. 10, pp. 2273–2279.

Hartman, M.L., O.S. Shirihai, M. Holbrook, G. Xu, M. Kocherla, A. Shah, J.L. Fetterman, M.A. Kluge, A.A., Frame, N.M. Hamburg and J.A. Vita, 2014, "Relation of Mitochondrial Oxygen Consumption in Peripheral Blood Mononuclear Cells to Vascular Function in Type 2 Diabetes Mellitus", *Vascular Medicine*, Vol. 19, No. 1, pp. 67–74.

Ignatenko, O., J. Nikkanen, A. Kononov, N. Zamboni, G. Ince-Dunn and A. Suomalainen, 2020, "Mitochondrial Spongiotic Brain Disease: Astrocytic Stress and Harmful Rapamycin and Ketosis Effect", *Life Science Alliance*, Vol. 3, No. 9, pp. e202000797.

Iommarini, L., S. Peralta, A. Torraco and F. Diaz, 2015, "Mitochondrial Diseases Part II: Mouse Models of OXPHOS Deficiencies Caused by Defects in Regulatory Factors and Other Components Required for Mitochondrial Function", *Mitochondrion*, Vol. 22, pp. 96–118.

Jahnke, V.E., J.H. Van Der Meulen, H.K. Johnston, S. Ghimbovschi, T. Partridge, E.P. Hoffman, and K. Nagaraju, 2012, "Metabolic Remodeling Agents Show Beneficial Effects in the Dystrophin-Deficient Mdx Mouse Model", *Skeletal Muscle*, Vo. 2, No. 1, pp. 16.

Joshi, C.N., C.R. Greenberg, A.A. Mhanni and M.S. Salman, 2009, "Ketogenic Diet in Alpers-Huttenlocher Syndrome", *Pediatric Neurology*, Vol. 40, No. 4, pp. 314–316.

Ju, J.S., S.I. Jeon, J.Y. Park, J.Y. Lee, S.C. Lee, K.J. Cho and J.M. Jeong, 2016, "Autophagy Plays a Role in Skeletal Muscle Mitochondrial Biogenesis in an Endurance Exercise-Trained Condition", *The Journal of Physiological Sciences: JPS*, Vol. 66, No. 5, pp. 417–430.

Kaiser, F., S. Krautwurst, S. Salentin, V.J. Haupt, C. Leberecht, S. Bittrich, D. Labudde and M. Schroeder, 2020, "The Structural Basis of the Genetic Code: Amino Acid Recognition by Aminoacyl-tRNA Synthetases", *Scientific Reports*, Vol. 10, No. 1, pp. 12647.

Kang, H.C., Y.M. Lee, H.D. Kim, J.S. Lee and A. Slama, 2007, "Safe and Effective Use of the Ketogenic Diet in Children with Epilepsy and Mitochondrial Respiratory Chain Complex Defects", *Epilepsia*, Vol. 48, No. 1, pp. 82–88.

Kardos, G.R., H.C. Wastyk and G.P. Robertson, 2015, "Disruption of Proline Synthesis in Melanoma Inhibits Protein Production Mediated by the GCN2 Pathway", *Molecular Cancer Research: MCR*, Vol. 13, No. 10, pp. 1408–1420.

Kartal, Ö., 2022, Further Characterization of Heart- and Skeletal Muscle-Specific Mitochondrial Aspartyl-tRNA Synthetase (DARS2) Knockout Mouse, M.S. Thesis, Boğaziçi University.

Khan, N.A., M. Auranen, I. Paetau, E. Pirinen, L. Euro, S. Forsström, L. Pasila, V. Velagapudi, C.J. Carroll, J. Auwerx and A. Suomalainen, 2014, "Effective Treatment of Mitochondrial

Myopathy by Nicotinamide Riboside, a Vitamin B3", *EMBO Molecular Medicine*, Vol. 6, No. 6, pp. 721–731.

Khan, N.A., J. Nikkanen, S. Yatsuga, C. Jackson, L. Wang, S. Pradhan, R. Kivelä, A. Pessia, V. Velagapudi and A. Suomalainen, 2017, "mTORC1 Regulates Mitochondrial Integrated Stress Response and Mitochondrial Myopathy Progression", *Cell Metabolism*, Vol. 26, No. 2, pp. 419–428.e5.

Kobilo, T., D. Guerrieri, Y. Zhang, S.C. Collica, K.G. Becker and H. van Praag, 2014, "AMPK Agonist AICAR Improves Cognition and Motor Coordination in Young and Aged Mice", *Learn Mem*, Vol. 21, No. 2, pp. 119-126.

Konovalova, S. and H. Tyynismaa, 2013, "Mitochondrial Aminoacyl-tRNA Synthetases in Human Disease", *Molecular Genetics and Metabolism*, Vol. 108, No. 4, pp. 206–211.

Koistinen, H.A., D. Galuska, A.V. Chibalin, J. Yang, J.R. Zierath, G.D. Holman and H. Wallberg-Henriksson, 2003, "5-Amino-Imidazole Carboxamide Riboside Increases Glucose Transport and Cell-Surface GLUT4 Content in Skeletal Muscle From Subjects with Type 2 Diabetes", *Diabetes*, Vol. 52, No. 5, pp. 1066–1072.

Lane, N. and W. Martin, 2010, "The Energetics of Genome Complexity", *Nature*, Vol. 467, 929–934.

Lehman, J.J., P.M. Barger, A. Kovacs, J.E. Saffitz, D.M. Medeiros and D.P. Kelly, 2000, "Peroxisome Proliferator-Activated Receptor Gamma Coactivator-1 Promotes Cardiac Mitochondrial Biogenesis", *The Journal of Clinical Investigation*, Vol. 106, No. 7, pp. 847–856.

Lefebvre, P., G. Chinetti, J.C. Fruchart and B. Staels, 2006, "Sorting Out the Roles of PPAR Alpha in Energy Metabolism and Vascular Homeostasis.", *The Journal of Clinical Investigation*, Vol. 116, No. 3, pp. 571–580.

Li, J.L., K.J. Tsai, C.C. Chan, T.Y. Lin, P.L. Chen, T.N. Guo, S.Y. Huang, C.H. Chen and C.H. Lin, 2021, "Mitochondrial Function and Parkinson's Disease: From the Perspective of the Electron Transport Chain", *Frontiers in Molecular Neuroscience*, Vol. 14, pp. 797833-797833.

Liang, H. and W.F. Ward, 2006, "PGC-1alpha: a Key Regulator of Energy Metabolism", *Advances in Physiology Education*, Vol. 30, No. 4, pp. 145–151.

Licari, E., L. Sánchez-del-Campo and P. Falletta, 2021, "The Two Faces of the Integrated Stress Response in Cancer Progression and Therapeutic Strategies", *The International Journal of Biochemistry and Cell Biology*, Vol. 139, pp. 106059.

Liu, W.J., L. Ye, W.F. Huang, L.J. Guo, Z.G. Xu, H.L. Wu, C. Yang and H.F. Liu, 2016, "p62 Links the Autophagy Pathway and the Ubiqutin-proteasome System upon Ubiquitinated Protein Degradation", *Cellular and Molecular Biology Letters*, Vol. 21 No. 1, pp. 1–14.

Mangum, J. E., J.P. Hardee, D.K. Fix, M.J. Puppa, J. Elkes, D. Altomare, Y. Bykhovskaya, D.R. Campagna, P.J. Schmidt, A.K. Sendamarai, H.G. Lidov, S.C. Barlow, N. Fischel-Ghodsian, M.D. Fleming, J.A. Carson and J.R. Patton, 2016, "Pseudouridine Synthase 1 Deficient Mice, a Model for Mitochondrial Myopathy with Sideroblastic Anemia, Exhibit Muscle Morphology and Physiology Alterations", *Scientific Reports*, Vol. 6, pp. 26202.

Margulis, L.S., 1970, "Recombination of Non-Chromosomal Genes in Chlamydomonas: Assortment of Mitochondria and Chloroplasts?", *Journal of Theoretical Biology*, Vol. 26, No. 2, pp. 337-342.

Merrill, G.F., E.J. Kurth, D.G. Hardie and W.W. Winder, 1997, "AICA Riboside Increases AMP-Activated Protein Kinase, Fatty Acid Oxidation, and Glucose Uptake in Rat Muscle", *The American Journal of Physiology*, Vol. 273, No. 6, pp. 1107-1112.

Metodiev, M.D., N. Lesko, C.B. Park, Y. Cámara, Y. Shi, R. Wibom, K. Hultenby, C.M. Gustafsson and N.G. Larsson, 2009, "Methylation of 12S rRNA is Necessary for in Vivo

Stability of the Small Subunit of the Mammalian Mitochondrial Ribosome", *Cell Metabolism*, Vol. 9, No. 4, pp. 386–397.

Mick, E., D.V. Titov, O.S. Skinner, R. Sharma, A.A. Jourdain and V.K. Mootha, 2020, "Distinct Mitochondrial Defects Trigger the Integrated Stress Response Depending on the Metabolic State of the Cell", *eLife*, Vol. 9, pp. 49178.

Milder, J. and M. Patel, 2012, "Modulation of Oxidative Stress and Mitochondrial Function by the Ketogenic Diet", *Epilepsy Research*, Vol. 100, No. 3, pp. 295–303.

Mitchell, P., 1961, "Coupling of Phosphorylation to Electron and Hydrogen Transfer a Chemi-Osmotic Type of Mechanism", *Nature*, Vol. 191, No. 4784, pp. 144-148.

Mitchell, P. and J. Moyle, 1967, "Chemi-Osmotic Hypothesis of Oxidative Phosphorylation", *Nature*, Vol. 213, No. 5072, pp. 137-139.

Moulis, M. and C. Vindis, 2017, "Methods for Measuring Autophagy in Mice", *Cells*, Vol. 6, No. 2, pp. 14.

Mourier, A., B. Ruzzenente, T. Brandt, W. Kühlbrandt and N.G. Larsson, 2014, "Loss of LRPPRC Causes ATP Synthase Deficiency", *Human Molecular Genetics*, Vol. 23, No. 10, pp. 2580–2592.

Murphy, J.L., T.E. Ratnaike, E. Shang, G. Falkous, E.L. Blakely, C.L. Alston, T. Taivassalo, R.G. Haller, R.W. Taylor and D.M. Turnbull, 2012, "Cytochrome C Oxidase-Intermediate Fibres: Importance in Understanding the Pathogenesis and Treatment of Mitochondrial Myopathy", *Neuromuscular Disorders: NMD*, Vol. 22, No. 8, pp. 690–698.

Nelson, D.L. and M.M. Cox, 2017, "Lehninger Principles of Biochemistry 7th", W.H. Free. Co.

Neupert, W. and J.M. Herrmann, 2007, "Translocation of Proteins into Mitochondria", *Annual Review of Biochemistry*, No. 76, pp. 723–749.

Nunnari, J. and A. Suomalainen, 2012, "Mitochondria: in Sickness and in Health", *Cell*, Vol. 148, pp. 1145-1159.

Nolfi-Donegan, D., A. Braganza and S. Shiva, 2020, "Mitochondrial Electron Transport Chain: Oxidative Phosphorylation, Oxidant Production, and Methods of Measurement", *Redox Biology*, Vol. 37, pp. 101674.

Peralta, S., S. Garcia, H.Y. Yin, T. Arguello, F. Diaz and C.T. Moraes, 2016, "Sustained AMPK Activation Improves Muscle Function in a Mitochondrial Myopathy Mouse Model by Promoting Muscle Fiber Regeneration", *Human Molecular Genetics*, Vol. 25, No. 15, pp. 3178-3191.

Pernas, L. and L. Scorrano, 2016, "Mito-Morphosis: Mitochondrial Fusion, Fission, and Cristae Remodeling as Key Mediators of Cellular Function", *Annual Review of Physiology*, Vol. 78, pp. 505–531.

Pfeffer, G. and P.F. Chinnery, 2013, "Diagnosis and Treatment of Mitochondrial Myopathies", *Annals of Medicine*, Vol. 45, No. 1, pp. 4–16.

Protasoni, M. and M. Zeviani, 2021, "Mitochondrial Structure and Bioenergetics in Normal and Disease Conditions", *International Journal of Molecular Sciences*, Vol. 22, No. 2, pp. 586.

Al Rawi, S., S. Louvet-Vallée, A. Djeddi, M. Sachse, E. Culetto, C. Hajjar, L. Boyd, R. Legouis and V. Galy, 2011, "Postfertilization Autophagy of Sperm Organelles Prevents Paternal Mitochondrial DNA Transmission", *Science*, Vol. 334, No. 6059, pp. 1144–1147.

Ruzzenente, B., M.D. Metodiev, A. Wredenberg, A. Bratic, C.B. Park, Y. Cámara, D. Milenkovic, V. Zickermann, R. Wibom, K. Hultenby, H. Erdjument-Bromage, P. Tempst, U. Brandt, J.B. Stewart, C.M. Gustafsson and N.G. Larsson, 2012, "LRPPRC is Necessary for Polyadenylation and Coordination of Translation of Mitochondrial mRNAs", *The EMBO Journal*, Vol. 31, No. 2, pp. 443–456.

Safdar, A., J.M. Bourgeois, D.I. Ogborn, J.P. Little, B.P. Hettinga, M. Akhtar, J.E. Thompson, S. Melov, N.J. Mocellin, G.C. Kujoth, T.A. Prolla and M.A. Tarnopolsky, 2011, "Endurance Exercise Rescues Progeroid Aging and Induces Systemic Mitochondrial Rejuvenation in mtDNA Mutator Mice*", Proceedings of the National Academy of Sciences of the United States of America*, Vol. 108, No. 10, pp. 4135–4140.

Scarpulla, R.C., R.B. Vega and D.P. Kelly, 2012, "Transcriptional Integration of Mitochondrial Biogenesis", *Trends in Endocrinology and Metabolism*, Vol. 23, No. 9, pp. 459–466.

Scheper, G.C., T. van der Klok, R.J. van Andel, C.G.M. van Berkel, M. Sissler, J. Smet, T.I. Muravina, S.V. Serkov, G. Uziel, M. Bugiani, R. Schiffmann, I. Kr¨ageloh-Mann, J.A.M. Smeitink, C. Florentz, R. van Coster, J.C. Pronk and M.S. van der Knaap, 2007, "Mitochondrial aspartyl-tRNA Synthetase Deficiency Causes Leukoencephalopathy with Brain Stem and Spinal Cord Involvement and Lactate Elevation", *Nature Genetics*, Vol. 39, No. 4, pp. 534–539.

Scialò, F., D.J. Fernández-Ayala and A. Sanz, 2017, "Role of Mitochondrial Reverse Electron Transport in ROS Signaling: Potential Roles in Health and Disease", *Frontiers in Physiology*, Vol. 8, pp. 428.

Seiliez, I., I. Belghit, Y. Gao, S. Skiba-Cassy, K. Dias, M. Cluzeaud, D. Rémond, N. Hafnaoui, B. Salin, N. Camougrand and S. Panserat, 2016, "Looking at the Metabolic Consequences of the Colchicine-Based in Vivo Autophagic Flux Assay", *Autophagy*, Vol. 12, No. 2, pp. 343–356.

Sharma, L., J. Lu and Y. Bai, 2009, "Mitochondrial Respiratory Complex I: Structure, Function and Implication in Human Diseases", *Current Medicinal Chemistry*, Vol. 16, No. 10, pp. 1266–1277.

Shutt, T.E. and M.W. Gray, 2006, "Bacteriophage Origins of Mitochondrial Replication and Transcription Proteins", *Trends in Genetics*, No. 22, Vol. 2, pp. 90–95.

Spelbrink, J., F.Y. Li, V. Tiranti, K. Nikali, Q.P. Yuan, M. Tariq, S. Wanrooij, N. Garrido, G. Comi, L. Morandi, L. Santoro, A. Toscano, G.M. Fabrizi, H. Somar, R. Croxen, D. Beeson, J. Poulton, A. Suomalainen, H.T. Jacobs, M. Zeviani and C. Larsson, 2001, "Human Mitochondrial DNA Deletions Associated with Mutations in the Gene Encoding Twinkle, a Phage T7 Gene 4-Like Protein Localized in Mitochondria", *Nature Genetics*, Vol. 28, pp. 223–231.

Sousa, J.S., E. D'Imprima and J. Vonck, 2018, J. R. Harris and E. J. Boekema (Editors), "Mitochondrial Respiratory Chain Complexes", *Membrane Protein Complexes: Structure and Function*, Vol. 87, pp. 167–227.

Suomalainen, A. and B.J. Battersby, 2018, "Mitochondrial Diseases: The Contribution of Organelle Stress Responses to Pathology", *Nature Reviews. Molecular Cell Biology*, Vol. 19, No. 2, pp. 77–92.

Suski, J.M., M. Lebiedzinska, M. Bonora, P. Pinton, J. Duszynski and M.R. Wieckowski, 2012, "Relation Between Mitochondrial Membrane Potential and ROS Formation", *Methods in Molecular Biology (Clifton, N.J.)*, Vol. 810, pp. 183–205

Taivassalo, T., N. De Stefano, J. Chen, G. Karpati, D.L. Arnold and Z. Argov, 1999, "Short-Term Aerobic Training Response in Chronic Myopathies", *Muscle & Nerve*, Vol. 22, No. 9, pp. 1239–1243.

Viscomi, C., E. Bottani, G. Civiletto, R. Cerutti, M. Moggio, G. Fagiolari, E.A. Schon, C. Lamperti and M. Zeviani, 2011, "In vivo Correction of COX Deficiency by Activation of the AMPK/PGC-1α Axis", *Cell Metabolism*, Vol. 14, No. 1, pp. 80–90.

Voos, W. and K. Röttgers, 2002, "Molecular Chaperones as Essential Mediators of Mitochondrial Biogenesis", *Biochimica et Biophysica Acta - Molecular Cell Research*, Vol. 1592, No. 1, pp. 51–62.

Wai, T. and T. Langer, 2016, "Mitochondrial Dynamics and Metabolic Regulation", *Trends in Endocrinology and Metabolism*, Vol. 27, No. 2, pp. 105–117.

Wenz, T., F. Diaz, B.M. Spiegelman and C.T. Moraes, 2008, "Activation of the PPAR/PGC-1alpha Pathway Prevents a Bioenergetic Deficit and Effectively Improves a Mitochondrial Myopathy Phenotype", *Cell Metabolism*, Vol. 8, No. 3, pp. 249–256.

Yılmaz. M., 2022, Preliminary Characterization of a Novel Mitochondrial Myopathy Mouse Model, M.S. Thesis, Boğaziçi University.

Yun, J. and T. Finkel, 2014, "Mitohormesis", *Cell Metabolism*, Vol. 19, No. 5, pp. 757–766.

Zalman, L.S., H. Nikaido and Y. Kagawa, 1980, "Mitochondrial Outer Membrane Contains a Protein Producing Nonspecific Diffusion Channels", *The Journal of Biological Chemistry*, Vol. 255, No. 5, pp. 1771–1774.

Zeviani M., 2008, "Train, train, train! No pain, just gain", *Brain*, Vol. 131, No. 11, pp. 2809–2811.

Zorova, L.D., V.A. Popkov, E.Y. Plotnikov, D.N. Silachev, I.B. Pevzner, S.S. Jankauskas, V.A. Babenko, S.D. Zorov, A.V. Balakireva, M Juhaszova, S.J. Sollott and D.B. Zorov, 2018, "Mitochondrial Membrane Potential", *Analytical Biochemistry*, Vol. 552, pp. 50–59.

Zweers, H., M.C.H. Janssen, S. Leij and G. Wanten, 2018, "Patients With Mitochondrial Disease Have an Inadequate Nutritional Intake", *Journal of Parenteral and Enteral Nutrition*, Vol. 42, No. 3, pp. 581–586.